INSIDE

Stadtwerke München GmbH
Innovative Energie Pullach
Karlsruher Institut für Technologie

Karlsruhe Institute of Technology

Verbundvorhaben: Induzierte Seismizität & Bodendeformation als Interferenzaspekte beim Betrieb von Geothermieanlagen in der süddeutschen Molasse – Untersuchungen zu einem ver-besserten Prozessverständnis im tiefen Untergrund und Maßnahmen zur Risikominimierung

INSIDE SEISMIC MONITORING APPROACHES: CAPABILITIES VERSUS COSTS

The authors are responsible for the content of this publication

Title:	INSIDE seismic monitoring approaches: Capabilities versus costs
Work package:	AP5.1: Kosten-/Nutzenanalysen der seismischen Aufzeichnungen
Milestone:	-
Due date:	-
Date:	-
Partner:	In charge: SWM, IEP, KIT
Contact person:	Jerome Azzola Email: jerome.azzola@kit.edu
Authors:	KIT: Jérôme Azzola, Emmanuel Gaucher
Version:	1.0

Version	Datum	Description of additions, changes, revisions
1.0	13.12.2024	First version

TABLE OF CONTENTS

LIST OF FIGURES

LIST OF TABLES

1   INTRODUCTION

This report evaluates the capabilities of different seismic monitoring approaches applied during the INSIDE project. These approaches cover traditional surface and borehole seismometers, a mini-array of geophones, and a Distributed Acoustic Sensing (DAS) system. This analysis uses as a prerequisite the catalogue of seismic events described in a separate report.

The monitoring concept developed in the frame of the project is briefly summarized in Section 2. Then, we present the monitoring results obtained from "unconventional" monitoring stations, i.e. a DAS station and a mini-array. We focus on comparing the ability of different technologies to detect seismic events (Section 3), characterize their source properties (Section 4). In addition, we evaluate the use of ambient noise for site characterization (Section 5). Finally, a cost comparison is provided, considering both installation and maintenance expenses for various monitoring solutions.

In the Section 7 of the report, the results are summarized, and recommendations are provided based on experience gained in INSIDE.

In the following, we use these conventions:

- DHDN / 3-degree Gauss-Kruger zone 4 ("GK4") coordinate system (EPSG 31468),
- Vertical coordinates are considered positive below MSL.

2   SEISMIC MONITORING OVERVIEW

2.1   THE MONITORING NETWORK

The INSIDE project focuses on to the seismic monitoring of the south of Munich, with a specific focus on the presently active Pullach and Schäftlarnstraße sites, and the upcoming Baierbrunn project. Figure 1 shows the monitoring sites used during the project. It includes:

- Four surface stations and one borehole station equipped with broadband geophones (red dots).
- Distributed Acoustic Sensing (DAS) in Buchenhain (blue diamond). Fiber optic cables (FOCs) have been installed and cemented in a 250 m deep monitoring well. Cables were additionally installed near surface, with a double 80 m long loop complementing the downhole installation. DAS on the combined FOC gives access to sensing points (SP) recording strain-rate (SR) time-series all over the length of the optical fiber.
- A mini-array of geophones, including nine independent geophones and data loggers, was installed in Siemens Park (blue diamond).
- To complete the dataset collected by the surface / borehole seismometers, we use recordings of the public stations part of the BayernNetz (green dots) (Department of Earth and Environmental Sciences, Geophysical Observatory, University of Munchen, 2001).

This report does not cover the six-month seismic monitoring conducted at the Schäftlarnstraße site using a DAS interrogator and a fiber optic cable cemented behind the casing of well TH3. This study is the subject of two open-access scientific publications (Azzola et al., 2023; Azzola and Gaucher, 2024), which detail the technical aspects of the experiment, the developed methodology and the monitoring results (in terms of seismic event detection, location and description). These articles also include an

analysis of the benefits associated with using DAS technology in this study. The main achievements in these study are included in the summary of the cost/benefits analysis.

Through the integration of various recording techniques in the field, it becomes possible to compare methods and articulate their respective advantages and disadvantages. This document focuses on the comparison of these different monitoring methods, instruments and configurations. In the later part of the report, "unconventional" monitoring stations refers to the Siemens Park and Buchenhain locations. The comparison focuses on following aspects:

- Evaluation of the strength of the seismic signals at each measurement point, in view of their detectability. This includes a comparison of observed Signal-to-Noise Ratios (SNR) within the frequency band used for event detection (5 to 40 Hz). Given that the various instruments yield different measurement types (such as ground vibrations or strain-rate for DAS), the use of this ratio facilitate the comparison of signals detectability.

- Evaluation of the capabilities in terms of event description. We focus on the possibility to describe the source of the detected seismic events from a single measurement station / instrument type, i.e. DAS or Mini-Array.

- The comparison also covers additional aspects, including financial considerations and the potential of the recordings for subsurface or site characterization infrastructures.
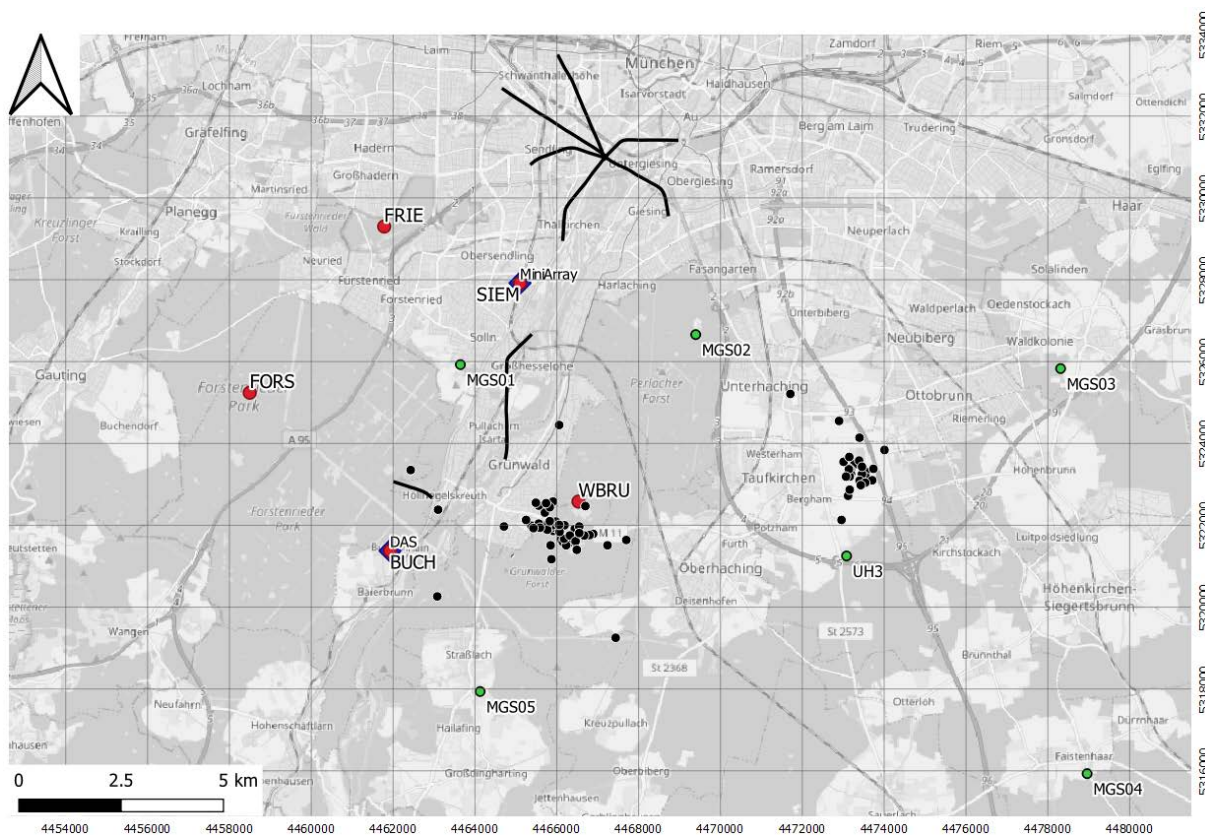
Figure 1: Overview of the monitoring network in the south of Munich. The black lines depict the projection on the surface of the borehole trajectories at the Pullach and Schäftlarnstraße sites. Red dots mark the locations of the INSIDE seismic monitoring stations, while green dots show the positions of the stations of the BayernNetz operated by the Geophysical Observatory Fürstenfeldbruck (GOF). The blue symbols show the location of "unconventional" monitoring stations, i.e. the mini array in Siemens Park and the DAS station in Buchenhain. Black dots show the epicenter of detected events (see Table 1)

2.2 CATALOG OF DETECTED EVENTS

To assess the benefit of DAS and the mini-array in view of the first two points mentioned previously, we focus on the data recorded around the onset times of the seismic events in the analyzed catalog. In Figure 1, we show the epicenters of these 79 events (black dots) detected with the seismometer network installed in the frame of the INSIDE project. These monitoring results are detailed in a dedicated open-access report.

The catalogue is summarized in Table 1. The table focuses also on a visual inspection of the DAS and mini-array recordings. The table delivers a qualitative evaluation of seismic signals across different types of instruments. The columns associated with the seismometer network indicate the feasibility of locating the event using the recordings of the five seismometer-stations deployed within the project (red dots in Figure 1) and categorizes the event origins. To evaluate the contribution of the borehole station SIEM, we use in Section 3.1 the entire catalog. The objective is to evaluate the sensitivity of the seismometer stations with respect to the background seismic noise conditions.

The last two columns of the table focus on DAS and mini-array. The columns focus on the period of recording of these "unconventional" stations", which is shorter than the seismometer stations. We assess whether the seismic signals observed on these specific dates on the DAS SPs (in Buchenhain) or on the stations of the mini-array (Siemens Park) allow for further signal processing, i.e. for event description. This includes the assessment of directionality of seismic waves (slowness and back azimuth) and the estimation of the event magnitude (local and / or moment magnitude).

Hence, we distinguish

- Events for which the signal is too weak, or the recordings are overshadowed by significant background noise, hindering signal identification and processing for event description (white background).
- Events for which the signal of interest is discernible on distinct traces, but the signal-to-noise ratio does not allow a consistent processing of the data subset (light green background).
- Events for which the signal-to-noise ratio allows for processing recordings to characterize the event (dark green background).

In section 3 and 4, we focus on the highlighted events to evaluate the capabilities of these "unconventional" stations compared to more traditional instrumentation types and configurations.

Table 1: Qualitative assessment of seismic signals across various instrument types, for each event detected by the seismometer network. The columns associated with the seismometer network show if the event location is possible from the recordings of the INSIDE network (dark green background) and the origin of the events, evaluated from a template analysis. We then highlight if the seismic signals observed on the DAS SPs (in Buchenhain) or on the stations of the mini-array (Siemens Park) at these specific dates allow the further processing of the signals, in view of event description.

■	Further processing is possible (e.g. location)
■	The signal is observed on channels / stations

| Trigger time (UTC) | INSIDE seismometer network | | Visible on | |
	Signal assessment	Origin (from templates)	DAS - BUCH	SIEM - mini-array
2021-03-05T21:56:23.24		Oberhaching		
2021-03-30T00:34:54.28		Oberhaching		
2021-06-04T14:55:57.89		Other		
2021-06-08T05:42:51.00		Oberhaching		
2021-06-18T16:40:02.38		Oberhaching		
2021-06-18T16:43:58.10		Oberhaching		
2021-06-18T17:01:45.22		Oberhaching		
2021-06-18T19:27:44.00		Oberhaching		
2021-06-19T01:40:37.00		Oberhaching		
2021-06-19T02:13:32.11		Oberhaching	**START**	
2021-10-22T17:55:02.50		Unterhaching		
2021-10-22T23:21:43.00		Unterhaching		
2021-10-23T03:05:39.60		Unterhaching		
2021-10-23T04:52:44.50		Unterhaching		
2021-10-23T18:51:16.60		Unterhaching		
2021-10-26T09:42:38.00		Unterhaching		
2021-10-28T21:49:11.80		Unterhaching		
2021-11-01T08:02:07.50		Unterhaching		
2021-12-03T15:24:11.50		Oberhaching		

Trigger time (UTC)	INSIDE seismometer network		Visible on	
	Signal assessment	Origin (from templates)	DAS - BUCH	SIEM - mini-array
2021-12-03T21:52:56.10		Unterhaching		
2022-01-18T23:52:53.50		Unterhaching		
2022-02-09T05:51:32.00		Unterhaching	No data	
2022-02-09T11:48:55.00		Unterhaching	No data	
2022-03-01T05:25:33.00		Unterhaching	No data	
2022-03-06T03:58:59.50		Oberhaching	No data	
2022-03-08T03:56:34.00		Oberhaching	No data	
2022-03-08T04:28:26.00		Oberhaching	No data	
2022-03-08T04:30:55.30		Oberhaching	No data	
2022-04-16T11:39:19.00		Oberhaching		
2022-04-23T12:10:58.00		Unterhaching		
2022-04-23T20:29:10.20		Unterhaching		
2022-05-21T22:24:11.50		Oberhaching		
2022-05-21T23:14:04.00		Oberhaching		
2022-05-21T23:48:19.50		Oberhaching		START
2022-05-26T20:51:30.00		Oberhaching		
2022-08-11T10:15:02.50		Oberhaching		
2022-09-07T00:56:43.00		Unterhaching		
2022-09-07T02:07:55.00		Unterhaching		
2022-09-25T14:48:05.50		Oberhaching		
2022-12-05T22:35:52.20		Unterhaching		
2022-12-09T03:21:41.50		Oberhaching		
2022-12-27T03:49:29.00		Oberhaching		
2023-01-15T21:08:04.00		Pullach (Th3)		
2023-02-25T15:35:00.20		Oberhaching		
2023-03-01T15:36:38.80		Oberhaching		

Trigger time (UTC)	INSIDE seismometer network		Visible on	
	Signal assessment	Origin (from templates)	DAS - BUCH	SIEM - mini-array
2023-03-06T08:52:15.30		Oberhaching		
2023-03-09T01:21:34.00		Oberhaching		
2023-04-22T23:06:43.10		Pullach (Th3)	No data	
2023-05-06T06:43:56.50		Oberhaching	No data	
2023-05-06T08:19:20.30		Oberhaching	No data	
2023-05-06T10:02:28.00		Oberhaching	No data	
2023-05-06T11:17:05.80		Oberhaching	No data	
2023-05-06T16:53:33.76		Oberhaching	No data	
2023-05-06T17:35:31.56		Oberhaching	No data	
2023-05-06T17:38:20.31		Oberhaching	No data	
2023-08-06T02:41:21.52		Oberhaching		
2023-08-06T02:51:48.98		Oberhaching		
2023-08-06T03:41:59.13		Oberhaching		
2023-08-06T03:43:01.05		Oberhaching		
2023-08-06T03:45:13.31		Oberhaching		
2023-08-06T03:50:34.72		Oberhaching		
2023-08-06T04:01:29.30		Oberhaching		
2023-08-06T04:25:01.66		Oberhaching		
2023-08-06T04:25:05.00		Oberhaching		
2023-08-06T04:36:51.28		Oberhaching		
2023-08-06T04:58:06.84		Oberhaching		
2023-08-06T04:58:39.66		Oberhaching		
2023-08-06T05:47:18.40		Oberhaching		
2023-10-17T03:09:50.70		Unterhaching		**END**
2023-10-24T00:43:56.32		Unterhaching		
2023-10-24T14:26:23.05		Unterhaching		

Trigger time (UTC)	INSIDE seismometer network		Visible on	
	Signal assessment	Origin (from templates)	DAS - BUCH	SIEM - mini-array
2023-10-27T01:56:06.43		Oberhaching		
2023-11-19T20:14:17.50		Unterhaching		
2023-11-20T04:31:22.90		Unterhaching		
2023-11-29T08:28:43.50		Unterhaching		
2023-11-29T08:32:06.60		Unterhaching		
2023-11-29T11:38:40.10		Unterhaching		
2023-11-29T12:01:32.60		Unterhaching		
2023-12-15T03:39:28.01		Oberhaching		

3 COMPARISON OF DETECTION CAPABILITIES

3.1 COMPARISON OF SEISMOMETER STATIONS

This section focuses first on the network of seismometers deployed as part of the INSIDE project. The analysis intends to evaluate the sensitivity of each station and compare the analysis to the noise measurements done after commissioning of the network.

Figure 2 represents statistically the distribution of estimated source-to-receiver distances, for each event listed in Table 1. A major part of the observed seismicity occurred near the Oberhaching and Unterhaching sites (e.g. Figure 1), southeast to the network of five INSIDE seismometers. In this context, Figure 2 along with the SNR observed at the station (see previous report) shows the benefit of the WBRU station (to lower extent, BUCH) for the detections reported in Table 1. Due to higher source-to-receiver distances, FORS and FRIE show lower detection capabilities.
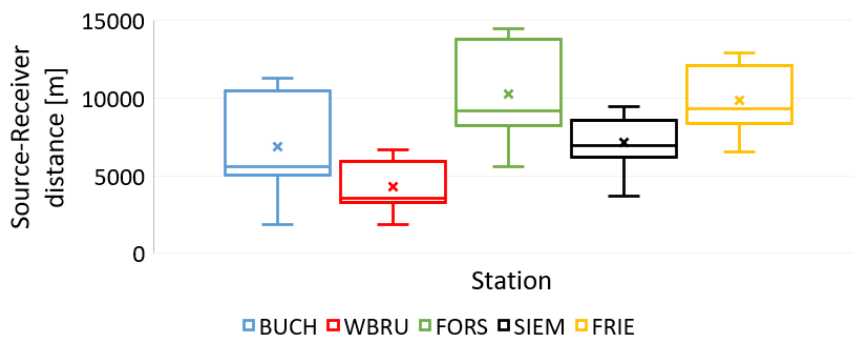
Figure 2: Statistical representation (boxplots) of the source to receiver distances computed for every event reported in Table 1. The whiskers extend from minimum to maximum value and the box extends from lower to upper quartile. The median is represented as a horizontal line and the mean as a cross.

However, the source to receiver distance plays a significant role in the observed SNR. As the major part of the observed seismicity originates from the sites at the margin of the network (southeast to the five stations), SNRs do not reflect the sensitivity of each station in an absolute way. For a more reliable comparison of the capabilities of the different seismometer station, we normalize the observed signal-to-noise ratio to the source-receiver distance. Hence, we derive a "detectability score" from SNR values and source-to-receiver distances. The normalization by source to receiver distance intends to reflect the recording (level of ambient noise) and installation conditions (sensitivity of the instruments).

Figure 3 shows the statistical distribution of the score computed for each analyzed event. It shows a significant contribution of the station in the Forstenrieder Park. Station FORS benefits from a low noise level, despite distance to observed events. The figure also evidences that the benefit of positioning the station in Siemensallee in a borehole is quite limited. This can be explained by a poor coupling of the sensor to the ground, leading to less sensitivity to the seismic signal and to higher background noise levels.

DETECTABILITY SCORE (SNR*DISTANCE TO EVENT)
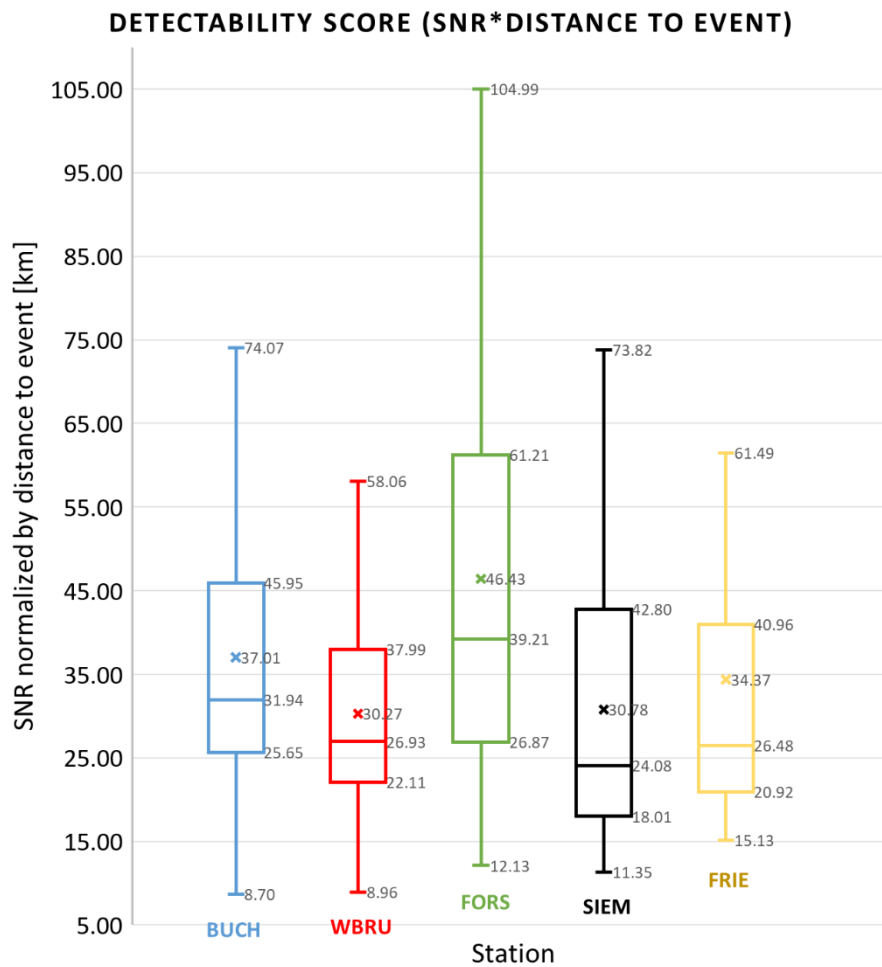
Figure 3: Statistical representation (boxplot) for every detected event of a detectability score, which is based on SNR values and source to receiver distances. The middle horizontal line indicates the median and the cross indicates the mean value. The whiskers indicate the upper and lower quartiles.

To compare the results derived from monitoring efforts (depicted in Figure 3) with the outcomes of noise analysis, we show in Figure 4 the distribution of I95 values that was computed from continuous recordings at each station. The metric characterizes the amplitude of background noise recorded by the seismometer in 30-minutes long data windows. I95 quantifies in each data-window the range of amplitudes defined by the 95th percentile, i.e. the limit that contains 95% of the recorded data. Here, we present the results from our analysis of a dataset comprising one month of continuous recordings.

On all three channels (panels (a) to (c)), the background noise evaluation shows that FORS is characterized by comparatively low background noise, which is also evidenced from the detectability score presented previously (Figure 3).
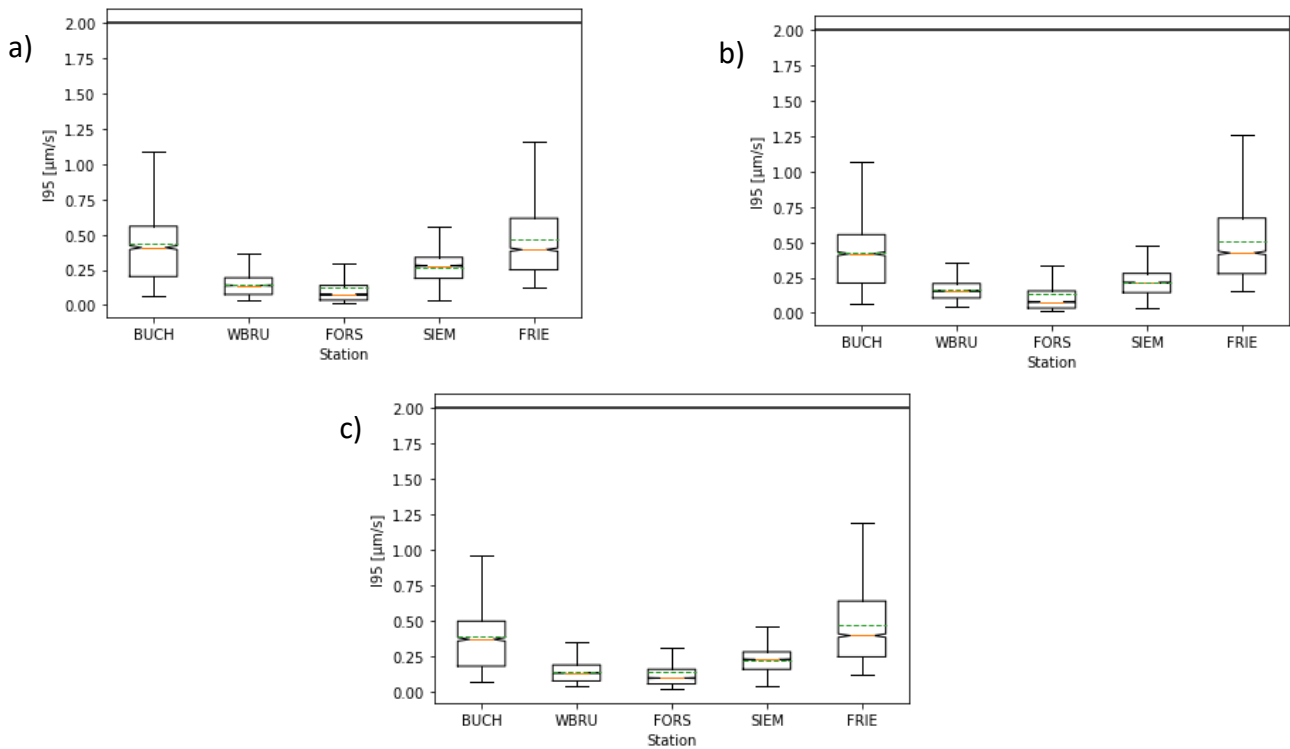
Figure 4: amplitude of ambient field vibrations presented as a statistical distribution of I95 values. For each station, the I95 values are evaluated within sliding 30-minutes data windows. The measurements are shown for the east components (a), the north components (b) and the vertical components (c). The bars extend to the extreme data points (min and max in the series of I95 values). The bottom and top edges of the frame indicate the 25th and 75th percentiles, respectively, and the orange line indicates the medians. The green dotted line represents the mean values. The notches indicate the standard deviation. The black line represents the threshold value of ±2 μm/s.

3.2 SIGNAL TO NOISE RATIO ON "NON-STANDARD" MONITORING STATIONS

The INSIDE monitoring network is made of a mix of measurement types: strain rate for DAS sensing points, and velocities for the mini array stations or seismometer stations. Hence, we use the Signal-to-Noise Ratio (SNR) observed on the measurement points of various instruments to evaluate and compare the detectability of seismic signals. We evaluate the possibly to improve the signal coherence and strength by applying processing techniques (filtering, stacking) to the recordings of multiple measurement points. As the mini-array and the DAS station are both approximately collocated to a seismometer station, we compare in both situations the measurement types without normalization to source-receiver distances, by comparing directly the observed SNR values.

3.2.1 MINI-ARRAY

Figure 5 shows the SNR observed in the 5-40 Hz frequency band for each detected event. We focus:

- on the channels of the SIEM borehole sensor (represented by the black line)
- on the mini-array stations, after the application of a band pass (B.P.) filter (red symbols).
- on the mini-array stations, after the application of a B.P. filter and after applying a shift and stack (beamforming, see Section 8.2) algorithm to the traces of all available stations (blue crosses).

The lines in the plot show all events detected during the recording period of the mini-array in Siemens Park. We classify the events based on the SNR observed on the SIEM seismometer.
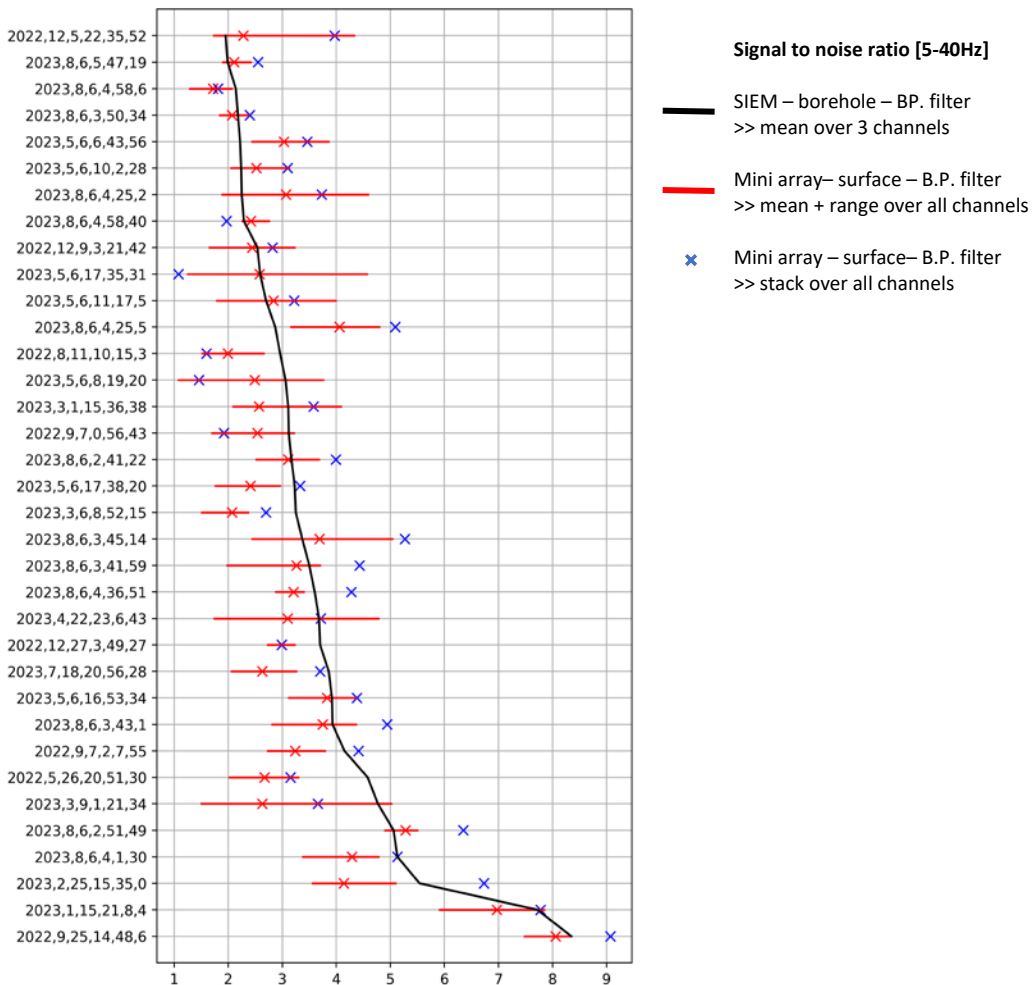
Figure 5: SNR values observed in the 5-40 Hz frequency band on the SIEM borehole sensor (depicted by the black line) and on the mini-array after application of a BP filter (red line). The Y-axis shows all events detected during operation of the mini-array in Siemens Park. The events are sorted based on the SNR observed on the SIEM seismometer.

In the target frequency band, the figure shows that applying beamforming to the mini-array recordings gives overall better SNR than applying a B.P. filter to the single borehole station SIEM. For events with low SNR on the SIEM channels, the average SNR over the mini-array geophones is also higher than for the borehole seismometer. It outlines the limited sensitivity of the borehole station, probably linked to a lack of coupling between the downhole sensor and the formation.

In Table 2, we assess the improvement in SNR after beamforming the mini-array traces for each event under analysis. The second column indicates the number of stations operational simultaneously during the seismic event, distinguished by a color code. The final column evaluates the how much the beamforming improves the SNR, compared to the case where we average the SNR observed on each B.P. trace. The percentage represents the relative improvement of SNR.

The table illustrates the variable benefit of beamforming, with an improvement in SNR that depends on the number of working stations, at the time of the seismic event. It underscores the operational challenges faced at the measurement stations, as the nine stations rarely recorded simultaneously. Additionally, frequent strong noise sources—such as those from the nearby train line—limit the processing capabilities.

Table 2: SNR improvement after processing of the mini-array recordings for each investigated event. Second column shows the number of operational stations at the time of the seismic event, which is highlighted by the color code. The last column evaluates the improvement of SNR from the average SNR observed on operational station, to the SNR observed on the stacked traces.

	Nbr. of stations	Average SNR [-]	SNR after stack [-]	Relative SNR improvement [%]
2022-09-25T14:48:06	6	8.06	9.07	13
2023-01-15T21:08:04	4	6.97	7.78	12
2023-08-06T02:51:49	5	5.28	6.35	20
2023-08-06T04:01:30	5	4.29	5.13	20
2023-02-25T15:35:00	9	4.14	6.73	62
2023-08-06T04:25:05	5	4.06	5.09	25
2023-05-06T16:53:34	7	3.83	4.38	14
2023-08-06T03:43:01	5	3.75	4.94	32
2023-08-06T03:45:14	5	3.69	5.27	43
2023-08-06T03:41:59	5	3.26	4.43	36
2022-09-07T02:07:55	6	3.24	4.41	36
2023-08-06T04:36:51	5	3.21	4.28	33
2023-08-06T02:41:22	5	3.11	3.99	28
2023-04-22T23:06:43	7	3.10	3.71	20
2023-08-06T04:25:02	5	3.07	3.73	21
2023-05-06T06:43:56	7	3.03	3.46	14
2022-12-27T03:49:27	6	2.99	2.99	0
2023-05-06T11:17:05	7	2.84	3.22	13
2022-05-26T20:51:30	7	2.67	3.15	18

3.2.2 DAS STATION

For the DAS monitoring station, we distinguish the surface and downhole part of the FOC as different processing methods can be applied to the measurements points identified along these sections (see Section 8.3 and 8.4).

Figure 6 focuses on the SPs distributed along the borehole cable. It shows the SNR values observed in the 5-40 Hz band for each detected event. We focus:

- on the channels of the BUCH borehole sensor (represented by the black line)
- on the strain-rate recordings of DAS SPs
    - after the application of a B.P. filter (blue line)
    - after the application of a B.P. filter and a f-k filter aiming at isolating plane waves propagating from bottom to top of the monitoring well (red symbols)
    - after applying a shift and stack algorithm, following the application of the B.P. and the f-k filter (green cross)
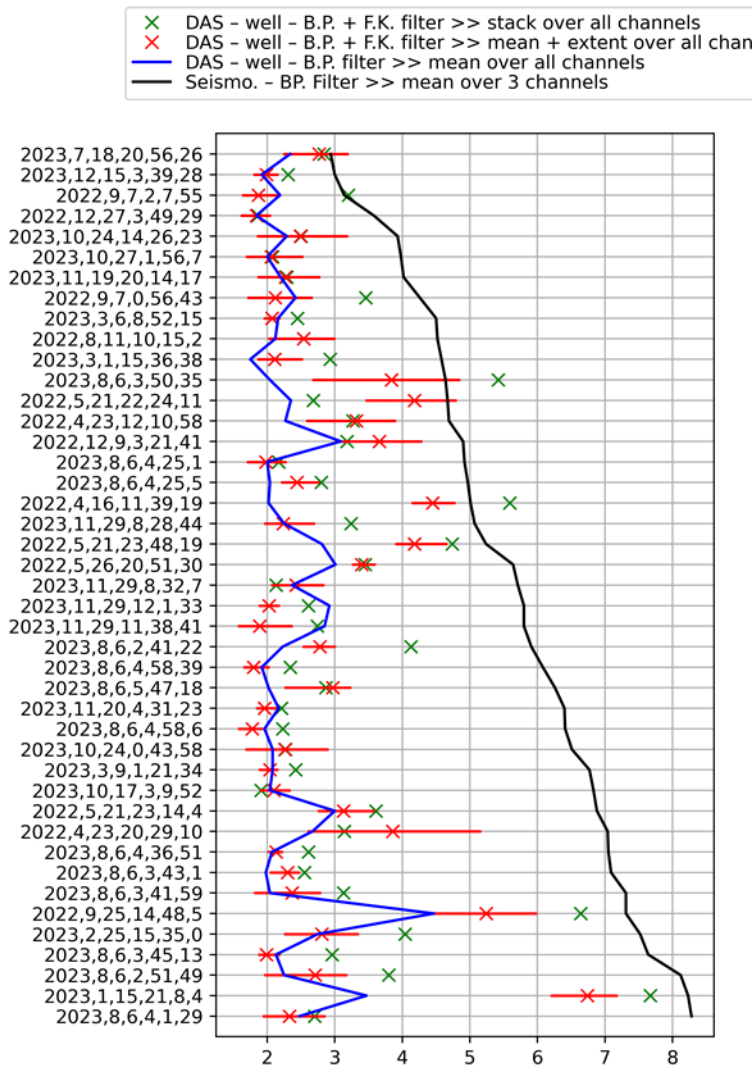
Figure 6: SNR values observed in the 5-40 Hz frequency band on the BUCH seismometer channels (depicted by the black line) and on the downhole DAS SPs after application of different processing methods. The Y-axis covers all seismic events detected during the operation of the DAS station. The events are sorted based on the SNR observed on the BUCH seismometer.

As in Figure 5 for the mini-array, the lines in the plot show the event detected during data recording. We classify the events based on the SNR observed on the BUCH seismometer. The figure illustrates that using frequency-wavenumber domain filtering leads to a substantial enhancement in signal strength. The improved SNR simultaneously results in an enhancement of inter-channel coherence. This coherence improvement is advantageous for accurately estimating delays between SPs, particularly in the context of applying a beamforming algorithm.

The methodology developed during the Schäftlarnstraße monitoring experiment and the related observations bring to a similar enhancement of SNR (see (Azzola and Gaucher, 2024)). The study also details the methodology developed to pick automatically P- and S- wave arrival times based on a narrow velocity-filter in the f-k domain. Moreover, (Azzola et al., 2023; Azzola and Gaucher, 2024) address the question of the increase of sensitivity to detection achieved with DAS in geothermal boreholes, with the detection of an event that would have been unnoticed from the surface seismometers.
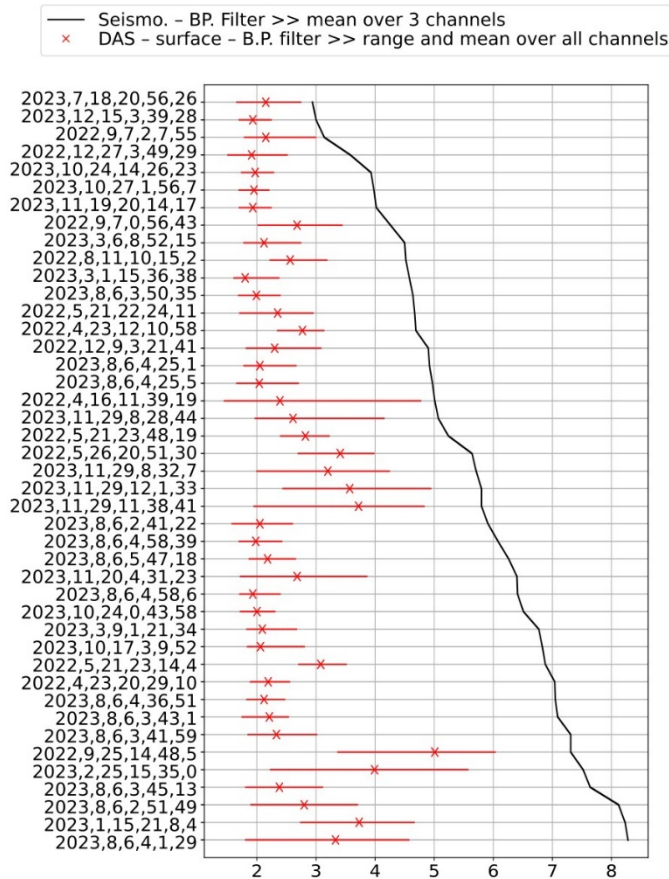
Figure 7: SNR values observed in the 5-40 Hz frequency band on the BUCH seismometer channels (depicted by the black line) and on the surface DAS SPs. The events are sorted based on the SNR observed on the BUCH seismometer.

Figure 7 focuses on the surface section, where we apply a single B.P. filter between 5 and 40 Hz. The figure shows the presence of elevated noise levels attributed to the anthropogenic activity surrounding the monitoring station, in the city center of Buchenhain. It also shows the limitations of DAS, which record data that are comparatively noisier than those recorded by standard seismometers (e.g. Lindsey et al. 2020).
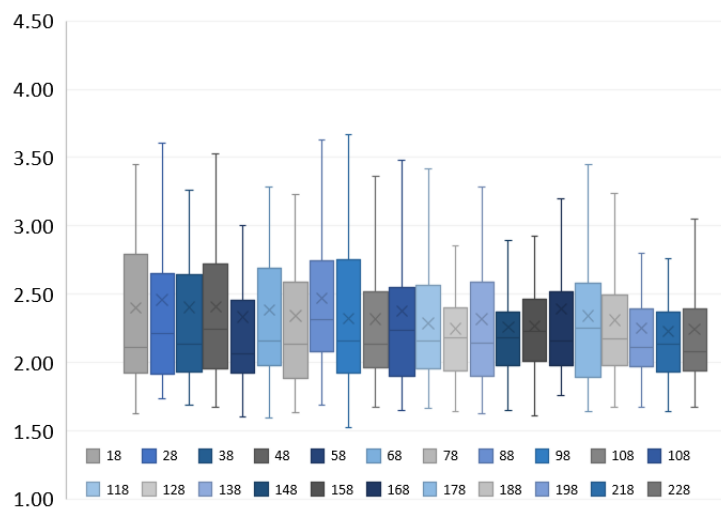
Figure 8: statistical distribution of SNR values observed in the 5-40 Hz frequency band on each downhole DAS SPs (from left to right) after application of a B.P. filter for all investigated events.

Figure 8 gives more insight into the SNR values measured along the downhole cable. It shows the statistical distribution of all SNR values measured at each SPs along the downhole FOC. The mean (crosses) and median (bars) values do not show an improvement of the SNR values with increasing depth and distance to surface anthropogenic noise. The figure does not highlight a clear increase of SNR with depth, suggesting that the borehole SPs do not significantly attenuate the anthropogenic noise at the investigated depths.

We observe oscillations along the cable. The downhole cable is cemented throughout the entire borehole, creating the most favorable condition for ensuring coupling of the optical fiber to the formation. However, Figure 8 might suggest that the strain transfer from ground to fiber varies along the cable, with locations more prone to capture the seismic signal. The centralizers installed along the PVC pipe used to lower the cable are spaced by 8 m. Hence, a clear connection to the position of the centralizers cannot be concluded.

3.3 NOISE MEASUREMENTS AT BUCHENHAIN

Figure 9 shows the temporal evolution of strain-rate amplitudes over one week and over the FOC route. The strain-rate amplitude is evaluated in consecutive 1-minute intervals, after applying a band pass filter in the 5 to 50 Hz frequency band, based on the 95th percentile of observed amplitudes. The figure shows persistent day/night variations on the recordings of the near-surface FOC loops, which is a pattern associated with anthropogenic background noise. The background strain-rate level occasionally reaches 30 $n\varepsilon.s^{-1}$ in day times. An attenuation is observed in the monitoring well (panel right), where lower background strain-rate amplitudes are observed. This observation suggests a reduction in surface noise, which contradicts the conclusion brought by the statistical distributions in Figure 8. Significant disturbances, with strain-rate exceeding 50 $n\varepsilon.s^{-1}$, are occasionally observed during the daytime, particularly on weekends. These signals propagate down to the well. They are attributed to the residents' presence near the measuring station.

Assessing the strength of the background strain-rate signal enables a comparison with the peak amplitudes recorded during a seismic event. For the January 15 event (see Sect. 8.3), maximum strain-rate amplitudes range from 50 nanostrain per second on the surface loop to around 70 nanostrain per second in the monitoring well
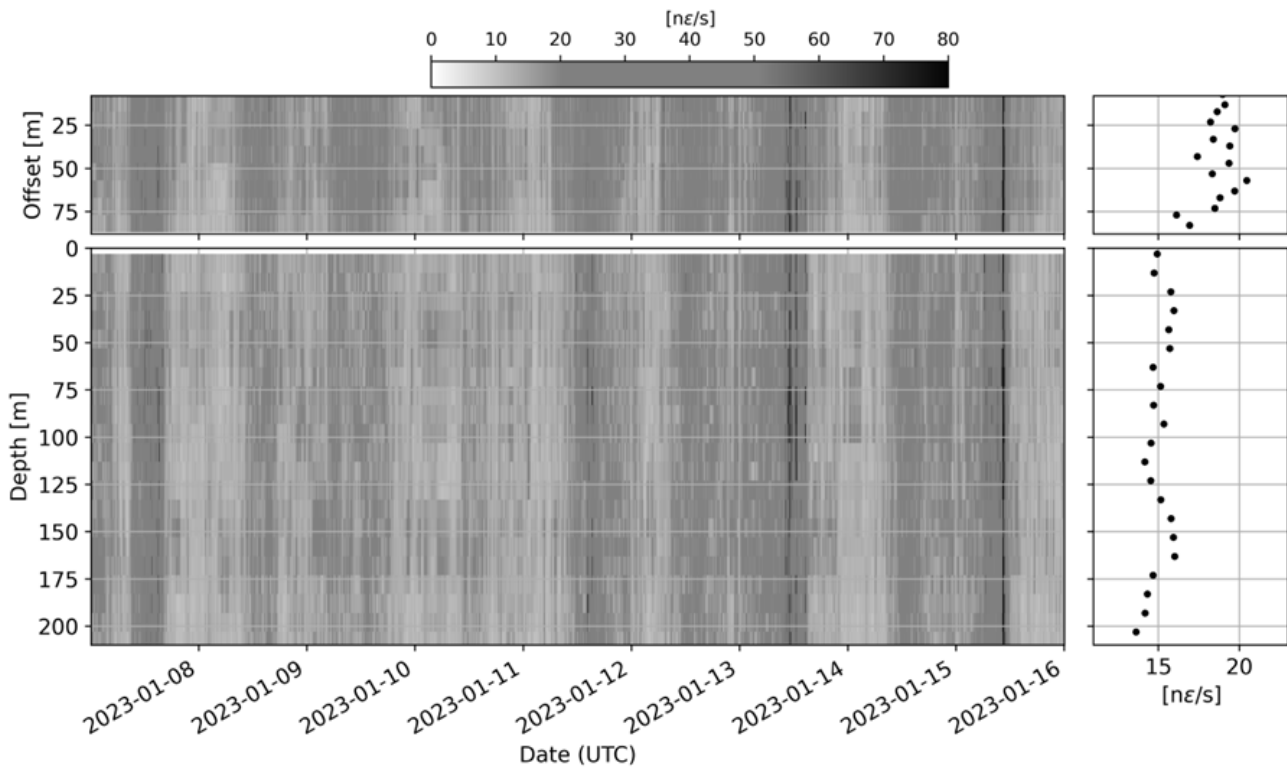
Figure 9: left -Temporal evolution of the strain-rate amplitudes over the FOC during the week preceding the January 15 seismic event. The color scale shows the 95th percentile of all strain rate values recorded over 1-minute-long windows. The time-series are plotted over offset on the near surface loop (top) and over depth in the monitoring well (bottom). Right - Spatial evolution along the optical fiber of the average over the 2023 – 01 – 11 of the strain-rate amplitude from the left panel.

The frequency distribution of background noise is typically evaluated by statistically analyzing Power Spectral Densities (PSDs) computed over successive data windows. The PSD can later be compared to reference noise models. (Peterson, 1993). The measurements is generally based on ground motion recording, typically velocity or acceleration. In Figure 10, we compare the median PSD computed from seismometer recordings to those obtained from DAS SPs located on the surface and in the well. Individual DAS PSDs are computed after converting the strain-rate spectra into acceleration. This conversion assumes that the background noise is predominantly composed of fundamental mode Rayleigh waves. The PSD computed from raw strain-rate data is multiplied by the phase velocity of Rayleigh waves, for every sampled frequency. The corresponding fundamental Rayleigh wave dispersion curve is modeled with the disba Python library (Luu, 2020) using a 1D-velocity model characteristic of the study area. Figure 10 shows that below 0.1 Hz, the signal is dominated by the signature of common-mode laser noise, with a peak occurring around 0.02 Hz. We observe no significant signature of the first microseismic peak in the median PSD of any DAS SP. At higher frequencies, between 10 and 100 Hz, we observe that both the seismometer and the DAS capture significant energy, likely linked to anthropogenic activities. Although the comparison between DAS and seismometer PSDs depends on the velocity model and the methods used for PSD calculation, we observe median PSDs differ by 7 dB between surface DAS SPs and the seismometer channel, in the targeted frequency range. For the in-well DAS SP, the difference is reduced to less than 5 dB. Hence, the influence of anthropogenic activities on the sensing points located in the monitoring well is reduced, as previously highlighted in Figure 9.
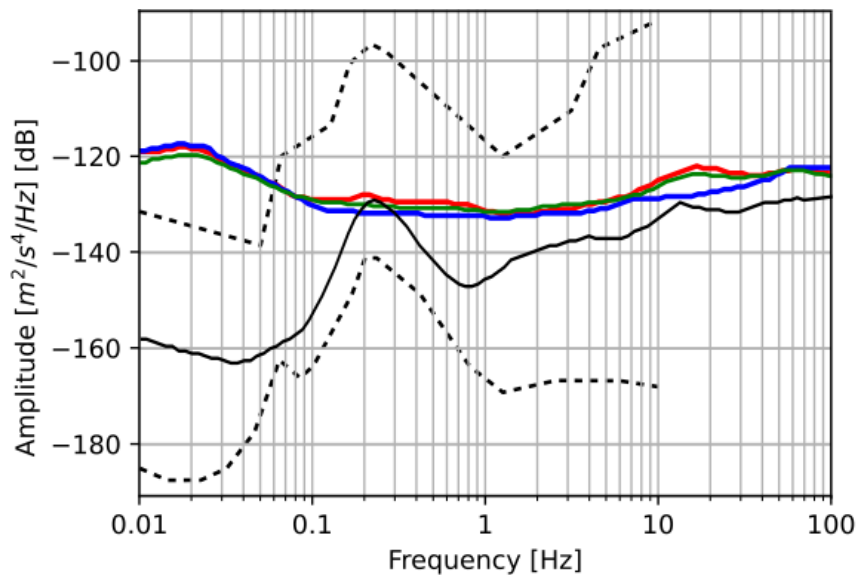
Figure 10: Comparison of median Power Spectral Densities (PSD) computed over the period of time displayed in panel (a). We compare the spectra obtained data from the BUCH HLZ channel (black line), from the DAS SP at an offset of 48 m on surface, and from the DAS SP at a depth of 10 m (green) and 200 m (blue) in the monitoring well. For comparison, the dashed lines show the new high and new low noise models (Peterson, 1993). Individual PSDs are computed using 30 minutes long windows. Additional details about the computation of the DAS PSD are included in the main text.

3.4 CONCLUSIONS

- The location of seismic stations used for event location is a critical factor in seismic monitoring. The results indicate that the station "WBRU" (and, to a lesser extent, "BUCH") exhibit high detection capabilities. This improved sensitivity is attributed to their proximity to the Oberhaching and Unterhaching sites.

- When analyzing the sensitivity of seismic stations independently from the location of detected events, the station in Forstenrieder Park stands out due to its low noise level. The term "sensitivity" here refers to the station's capacity to detect seismic signals amidst background noise, regardless distance to seismic events. A lower noise level enhances the station's ability to discern and capture relevant seismic events.

- The benefit of the borehole station in Siemensallee is found to be quite limited. This limitation is likely attributed to poor coupling of the sensor, i.e. a limited efficiency with which the sensor is physically connected to the surrounding medium. In the target frequency band, stacking seismic data over the mini-array yields superior results compared to the borehole station. The mini-array's configuration proves advantageous for signal enhancement, making it a preferred choice for seismic monitoring.

- A particular asset of the DAS station is the vertical monitoring well, which allows application of f-k filtering techniques. This processing method is identified as a beneficial technique for enhancing the strength of signals recorded in the downhole section of the DAS-station.

- Using DAS from behind a flowing geothermal well in Schäftlarnstraße proved beneficial to the sensitivity of the monitoring network and complemented the seismometer network.

- A slight reduction of the impact of anthropogenic noise on sensing points located in the monitoring well is observed from noise measurements at the Buchenhain station in the targeted frequency range.

4 COMPARISON OF SOURCE DESCRIPTION CAPABILITIES

The capabilities of the mini-array (see Section 4.1) and of the DAS array (see Section 4.2) are tested in terms of event description using the recordings associated with the events listed in Table 1. If the SNR observed on independent SPs along the FOC or on mini-array geophones is sufficient (see green background in Table 1), we analyze the recordings according to the workflows described in Section 0. These processing steps aim to achieve the objectives of seismic monitoring. From a single measurement type / configuration, we aim to:

- Localize the source of seismic events from the back azimuth of measured wave fields (and the incidence, using the DAS station),
- Describe the dynamic of the seismic source, in particular estimate the moment magnitude.

4.1 MONITORING RESULTS AT THE SIEMENS PARK MINI-ARRAY

The Siemens Park mini-array is made of nine stations dispatched in the Siemens Park in a radius of approximately 5 km. Each station is equipped with a 3-component geophone recording at a frequency of 200 Hz.

Figure 11: Maps focusing on the monitoring instruments deployed near the Siemens Park.

In the context of array processing, wavenumber differences affect the array's ability to resolve and distinguish between different seismic waves (see Section 8.1). Figure 12 shows the array transfer function calculated with the geometry of the mini-array in Siemens Park. It shows that the main lobe is narrow, notably in comparison to the array transfer function for the Buchenhain station (Figure 14), due to the network's much wider aperture. This results in a higher resolution in measuring apparent velocities. However, the array shows differences in resolution for different azimuths, which are due to its geometry. The numerous side lobes in the transfer function are due to the greater distances between the different sites in the array.
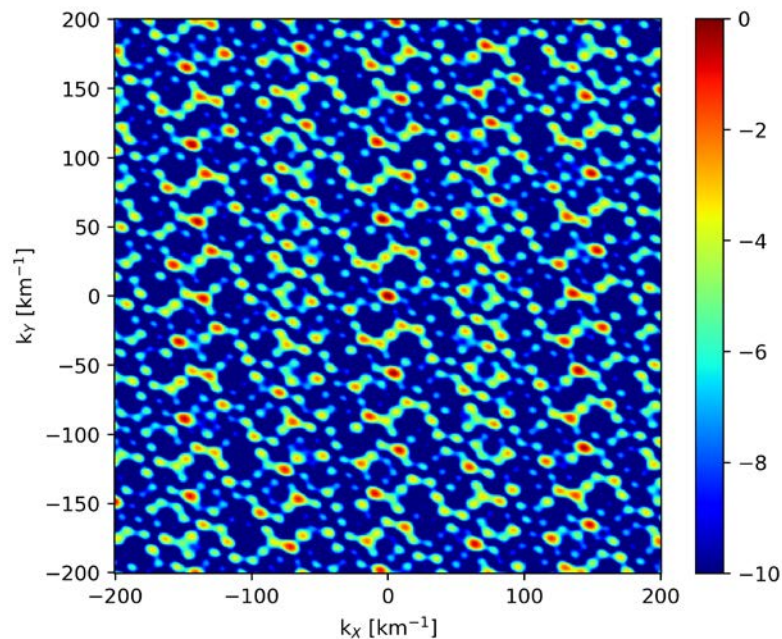
Figure 12: Transfer function of the array made of 9 geophones in the Siemens Park. The figure shows the relative power of the array response normalized with its maximum as a function of wavenumber difference.

Table 3 shows the results of beamforming for seismic events observed on the Siemens Park mini-array. The table includes the SNR values from Table 2. We show the back-azimuth (BAZ) estimated at maximum beam power and the associated slowness components (s_{XX} and s_{YY}). The table also includes a comparison of the resulting BAZ values with those computed from the epicenters obtained from the recordings of the seismometer network (see Figure 1). Additional details about the methodology used to obtain the results are presented in Section 8.2 using an example of event.

The table shows that the BAZ estimated from the mini-array are mostly consistent with network locations. The mini-array BAZ measurements falling into a ±10 % error margin compared to the seismometer network measurements are highlighted with a green background. We observe a good consistency in the mini-array measurement despite the operating challenges illustrated by the third column:

- - Frequent strong local noise sources, illustrated by the proximity of the network to the railway line, which can pollute recordings associated with a seismic event.
- Rarely simultaneous recording of nine stations, which shows an impact on the SNR improvement consecutive to stacking.

.

Table 3: Beamforming results for seismic events observed on the Siemens Park mini-array and comparison of resulting back azimuth (BAZ) with the measurements obtained from the seismometer network. The light green background highlights events for which the estimated back azimuth is particularly consistent with the one estimated with seismometer data.

Origin time (UTC)	Average SNR [-]	SNR after stack [-]	Estimated BAZ [°]	Expected BAZ [°] - from KIT locs	Estimated [km/s] - S_{XX}	slowness [km/s] - S_{YY}
2022-09-25T14:48:4.348592	8.06	9.07	169	168	-0.09	0.27
2023-01-15T21:08:3.068068	6.97	7.78	211	196	0.09	0.15
2023-08-06T02:51:47.945934	5.28	6.35	138	165	-1.24	1.36
2023-08-06T04:01:28.269025	4.29	5.13	162	165	-0.09	0.27
2023-02-25T15:34:58.819246	4.14	6.73	157	161	-0.09	0.21
2023-08-06T04:25:4.035632	4.06	5.09	157	168	-0.76	1.79
2023-05-06T16:53:32.829994	3.83	4.38	172	172	0.03	0.21
2023-08-06T03:43:0.020600	3.75	4.94	150	167	-0.94	1.61
2023-08-06T03:45:12.346705	3.69	5.27	153	169	-0.58	1.12
2023-08-06T03:41:58.153674	3.26	4.43	172	170	-0.03	0.21
2022-09-07T02:07:51.067636	3.24	4.41	115	116	-0.21	0.03
2023-08-06T04:36:50.235289	3.21	4.28	130	165	-1.18	1.00
2023-08-06T02:41:20.424901	3.11	3.99	163	165	-0.52	1.73
2023-04-22T23:06:42.109115	3.10	3.71	188	205	0.03	0.21
2023-08-06T04:25:0.594332	3.07	3.73	171	165	-0.15	1.00
2023-05-06T06:43:55.676742	3.03	3.46	299	174	0.27	-0.15
2022-12-27T03:49:26.649807	2.99	2.99	94	161	-1.30	0.09
2023-05-06T11:17:4.811351	2.84	3.22	113	171	-0.64	0.27
2022-05-26T20:51:28.885347	2.67	3.15	149	170	0.09	0.15

4.2 MONITORING RESULTS AT THE BUCHENHAIN DAS STATION

The measurement station includes two loops of FOC installed near surface. We observe an offset between the sensing points on both loops, which densifies the network of SPs. Figure 13 shows the layout of the DAS station.
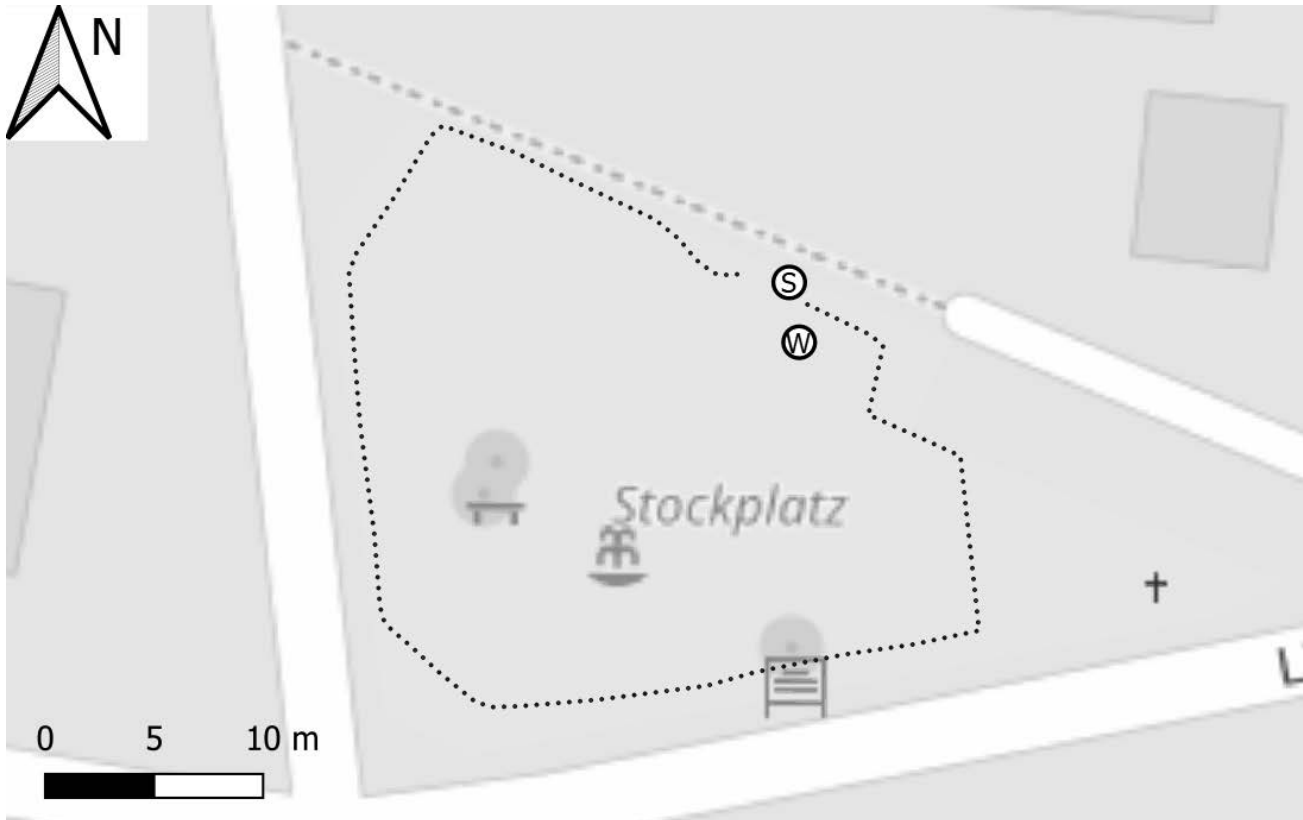
Figure 13: Buchenhain DAS station with the location of the FOC near surface (black dots), the BUCH seismometer (S) and the monitoring well (W).

Figure 14 shows the array transfer function calculated if considering that each DAS SP on the surface loops is occupied by a seismometer. The geometry of the surface DAS array yields a good azimuthal resolution, with an isolated main lobe resulting from the closely spaced SP, implying low differences in resolution for different azimuths. Nevertheless, this array cannot distinguish between waves with small wavenumber differences because of the small aperture, as can be seen in the relatively wide main lobe of the transfer function.

Higher frequency waves have shorter wavelengths, and thus larger wavenumbers. To accurately sample and resolve these waves, the sensor spacing needs to be small enough to capture the high spatial frequency components. This high spatial resolution means that the array can distinguish between closely spaced features in the wave front, effectively resolving high-frequency signals. Arrays with smaller sensor spacing (high spatial resolution) are therefore better at resolving these higher wavenumbers. Conversely, low-frequency waves with longer wavelengths require arrays with larger apertures to be resolved effectively. Larger apertures are necessary to resolve these long wavelengths because they provide a larger baseline over which the wave front can be sampled.
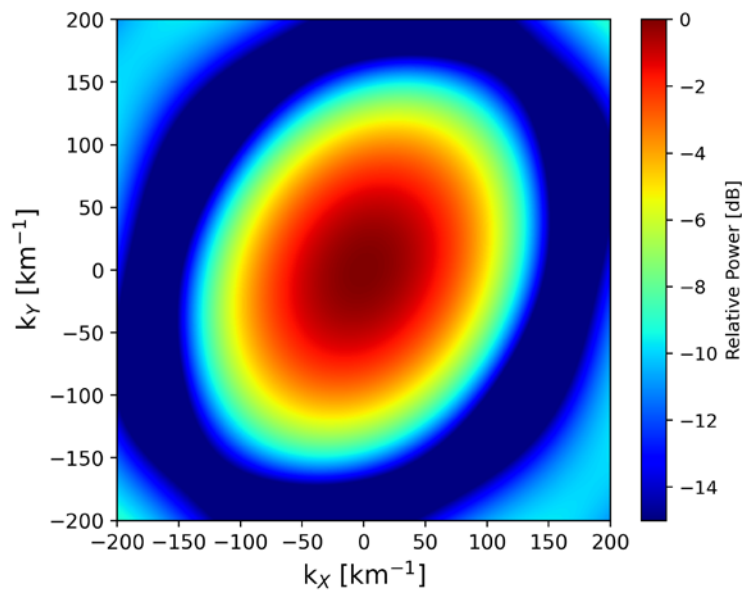
Figure 14: Relative power of the array response normalized with its maximum as a function of wavenumber difference. The computation of the array transfer function assumes that each DAS SP is replaced by a seismometer, i.e., we neglect effects related to the directivity of the wavefield and the geometry of the FOC.

Table 4 shows the results of beamforming applied to the recordings of the DAS station, for all compatible events. Compared to the mini-array in Siemens Park, the fit between the results from seismometer and DAS measurements is more contrasted, with the pale green background showing the events for which we obtain a significant fit. Lower distant of the station to the hypocenter (pale red background), higher frequency content of the analyzed signal (example of the January 15 event), and higher SNR on the surface recordings yield better results. In particular, the 15 January 2023 event is an example of an event for which the design of the DAS SP array is suitable for event description.

Table 4 includes the incidence and moment magnitude estimated from the downhole SPs. The combination of downhole and surface fiber optic cable is a significant advantage of the DAS station, facilitating the implementation of processing techniques for automatic detection of P and S wave onset times, assessment of source-to-receiver distance, and further characterization of the seismic source.

The workflow described in Section 8.4 for seismic source description also allows evaluating the reliability of ground vibration measurements provided by DAS. For example, Figure 30 compares for a specific event the waveforms recorded by DAS to the one collected by the surface seismometer. The close alignment in terms of phase and amplitude suggests that DAS accurately captures ground vibration measurements in the well, enabling the evaluation of seismic source characteristics.

Table 4: Seismic event characterization with DAS data at the Buchenhain station and comparison with measurements obtained from the seismometer network. The columns detail, for each event with an average SNR higher than 2.0, some general characteristics. This includes the event origin time (UTC referenced), the average SNR observed on the surface loop, the most significant frequency evaluated from Continuous Wavelet Transform (CWT), the distance between the station and the hypocenter from the seismometer network with the red background classifying the values from lowest (light) to largest (dark) distances. Then, we detail the ray parameters (incidence INC, back azimuth BAZ) and moment magnitude (MW) obtained with the seismometer network. Then, we focus on the results from the DAS station. Rows with light green background indicate events for which the back azimuth is within the range of estimates calculated from the extent of the 68% confidence interval around the most likely hypocentre computed from the seismometer network.

Origin time (UTC)	Average SNR [-]	Main frequency [Hz]	Distance to epicenter [km]	Network			DAS station		
				INC	BAZ	MW	INC	BAZ	MW
2022-04-23T12:10:55.336377	2.6	16	11.8	74	82	1.02	75	91	0.58
2022-04-23T20:29:7.976419	2.2	15	11.5	73	83	1.00	77	96	0.57
2022-05-21T22:24:10.739096	2.4	21	4.5	50	83	0.60	48	80	0.60
2022-05-21T23:14:02.904272	2.9	20	6.0	51	84	0.54	48	92	0.59
2022-05-21T23:48:18.251352	2.8	19	5.8	50	83	0.70	51	94	0.59
2022-05-26T20:51:28.885347	3.3	25	5.2	49	77	0.43	47	86	0.48
2022-08-11T10:15:1.401202	2.7	18	5.3	49	76	0.52	44	74	0.52
2022-09-07T00:56:39.787125	2.4	17	11.9	73	80	0.90	58	70	0.59
2022-09-07T02:07:51.067636	2.2	17	11.7	76	77	0.69	69	62	0.53
2022-09-25T14:48:04.348592	5.0	26	5.6	49	75	1.04	46	82	1.00
2023-01-15T21:08:03.068068	**3.7**	**37**	**3.7**	29	44	0.40	29	44	0.40
2023-02-25T15:34:58.819246	4.0	24	6.1	56	86	0.80	52	84	0.80
2023-03-06T08:52:13.846851	2.1	21	5.7	57	86	0.68	49	84	0.66
2023-03-09T01:21:32.721089	2.8	26	5.0	48	76	0.80	47	73	0.53
2023-08-06T02:41:20.424901	2.1	24	5.9	51	84	0.54	37	95	0.43
2023-08-06T02:51:47.945934	2.8	25	5.9	51	84	0.34	49	76	0.36
2023-08-06T03:41:58.153674	2.3	23	5.3	51	82	0.70	49	79	0.64
2023-08-06T03:43:00.020600	2.6	22	5.7	51	83	0.80	46	74	0.57
2023-08-06T03:45:12.346705	2.4	26	5.3	50	82	0.80	35	68	0.63
2023-08-06T04:01:28.269025	3.6	28	5.9	51	83	0.50	44	83	0.62

Origin time (UTC)	Average SNR [-]	Main frequency [Hz]	Distance to epicenter [km]	Network			DAS station		
				INC	BAZ	MW	INC	BAZ	MW
2023-08-06T04:25:00.594332	2.1	25	5.7	52	84	0.44	38	70	0.38
2023-08-06T04:36:50.235289	2.6	20	5.8	50	84	0.68	48	84	0.39
2023-08-06T05:47:17.409564	2.2	20	5.3	51	83	0.70	52	87	0.45
2023-10-17T03:09:49.836912	2.1	18	12.1	71	82	0.80	80	86	0.58
2023-10-24T00:43:55.443190	2.0	15	11.7	74	80	0.76	60	68	0.61
2023-11-20T04:31:21.059110	2.9	16	12.0	72	82	1.17	66	85	1.20
2023-11-29T08:28:41.596065	2.6	16	12.3	71	81	1.00	56	90	0.67
2023-11-29T08:32:4.646095	3.4	16	12.4	73	81	1.08	62	88	1.20
2023-11-29T11:38:38.296095	3.6	14	12.2	72	80	1.40	75	92	1.40
2023-11-29T12:01:30.766147	3.2	15	12.2	72	81	1.00	80	86	1.00

4.3 CONCLUSIONS

For locating seismic events and estimating source parameters, the comparison of measurement instruments and installed configurations leads to the following conclusions.

- The monitoring results from the Siemens Park mini-array are consistent with those from the seismometer array. Operational difficulties related to maintenance reliance limit its capabilities, particularly in terms of signal enhancement.
- The design of the DAS station results in three-dimensional sensing capacities, analogue to a 3C sensor. Its extent allows estimating back azimuth and incidence of the wave field from a single station. The estimate is consisting with the measurements obtained from the entire seismometer network for seismic events which are compatible with the sensitivity / resolution of the array of DAS SP.
- Compared to the mini-array in Siemens Park, the fit between the results from seismometer and DAS measurements in Buchenhain is more contrasted. This is also related to the characteristics of the seismic events recorded on the DAS array, which are relatively distant to the station. The results are compatible with those of the seismometer network under conditions: high SNR and high frequency content of the signals. The capabilities of the Siemens Park and Buchenhain arrays for beamforming are strongly tied to the geometry of the respective arrays. The geometry of the surface DAS array yields a good azimuthal resolution, with an isolated main lobe resulting from the closely spaced SP. Unlike the Siemens Park mini-array, the Buchenhain DAS array cannot distinguish between waves with small wavenumber differences, as can be seen in the main lobe of the transfer function. Higher frequency waves have shorter wavelengths, and thus larger wavenumbers. The Buchenhain DAS array, with smaller sensor spacing (high spatial resolution) is better at resolving these higher wavenumbers. Conversely, low-frequency waves with longer wavelengths require arrays with larger apertures, such as the mini-array in Siemens Park, to be resolved effectively.
- The application of DAS on a vertical fibre-optic cable over 250 m (Buchenhain) to 700 m (Schäftlarnstraße) is advantageous for the application of advanced filtering techniques (e.g. velocity-filters in the frequency-wavelength domain) as well as for the automated extraction of P- and S-wave onset times and the detailed description of seismic events.
- The DAS station independently gives access to several observational capabilities, since a single cable can be interrogated by several interrogators. This gives virtually access to distributed acoustic (DAS) measurements but also static deformation measurements (DSS). The later measurements are not discussed in the report.

5 SITE CHARACTERIZATION CAPABILITIES

To extend beyond standard seismic monitoring practices, we consider the recordings collected by the different instruments and infrastructures for the characterization of subsurface properties and surface responses. The results collected from such analysis can be used for refining velocity structures and play a crucial role in predicting the amplification and propagation patterns of seismic waves.

5.1 SPECTRAL RATIOS AND FUNDAMENTAL FREQUENCIES

We use the GEOPSY software (Wathelet et al., 2020) to calculate Horizontal-to-Vertical (H/V) spectral ratios at the various monitoring sites, taking into account the diversity of instrumentation types. This analysis allows us to evaluate the characteristics of ground motion in terms of the ratio between horizontal and vertical components across different seismic monitoring instruments (see Section 8.6).

5.1.1 MINI-ARRAY

We use data recorded by the mini-array on January 22 (Sunday), during a period when all nice stations within the mini-array were recording simultaneously. We process a 30 minute long data subset, recorded after 2 am (UTC), as we suppose that anthropogenic noise is lowest during this period (including, less activity on the railways). The aim is to work towards optimal recording conditions for ambient vibration recordings, specifically, achieving omnidirectional and equipotential recording of uncorrelated background noise. The processing steps are detailed in Section 8.6 with the associated theoretical background.

Figure 15 shows the results obtained for each station part of the mini-array. The black curve representing the geometrically averaged H/V results show a significant peak around 17 Hz. This peak represents the fundamental frequency f_0, which characterizes the site response and subsurface (see Section 8.6) and described the frequency at which the site responds most strongly to ground motion. The peak is found to exceed a ratio of 2, which is considered as a threshold for the peak to be significant (Bard et al., 2008). This result is consistent from one station to the other, expected for the station "S5" which is closest to a main road. In addition, the dashed lines representing the standard deviation over individual curves highlight the consistency of the measurements.

Figure 16, which summarizes the H/V results for all the investigated stations, shows no significant spatial variability over the surface covered by the mini-array.

Considering a fundamental frequency f_0 = 17 Hz, and assuming V_S, the average shear-wave velocity in the soft layer, to be equal to 800 m/s (see for example Figure 21), we measure H, the thickness of the soft layer, of around 12 m.
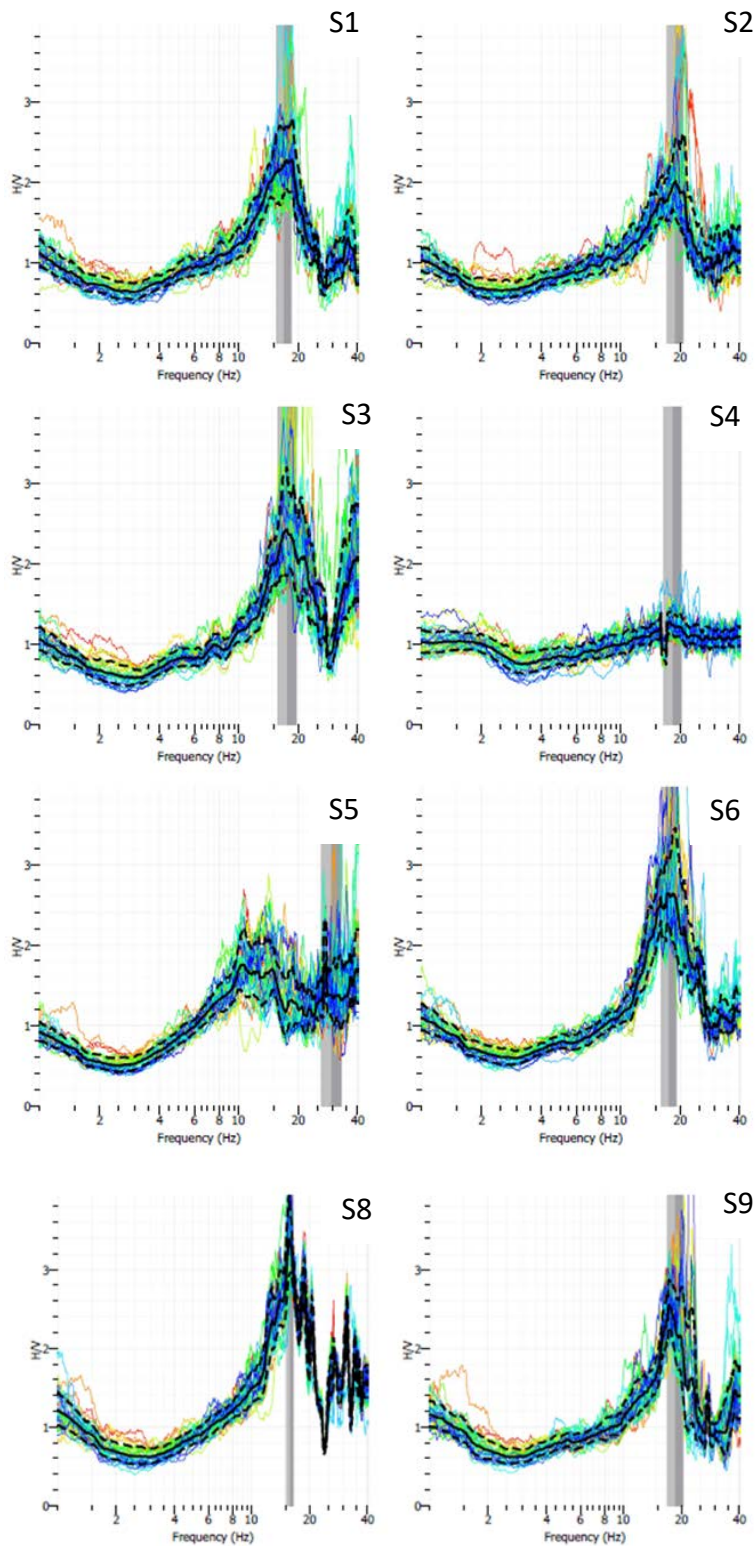
Figure 15: H/V curves computed from 30-minute-long data subset recorded at each station of the mini-array. Each colored curve represents the H/V ratio computed in sliding window. The black curve represents H/V geometrically averaged over all colored individual H/V curves. The two dashed lines represent the H/V standard deviation. The grey area represents the averaged peak frequency and its standard deviation. The frequency value is at the limit between the dark grey and light grey areas.
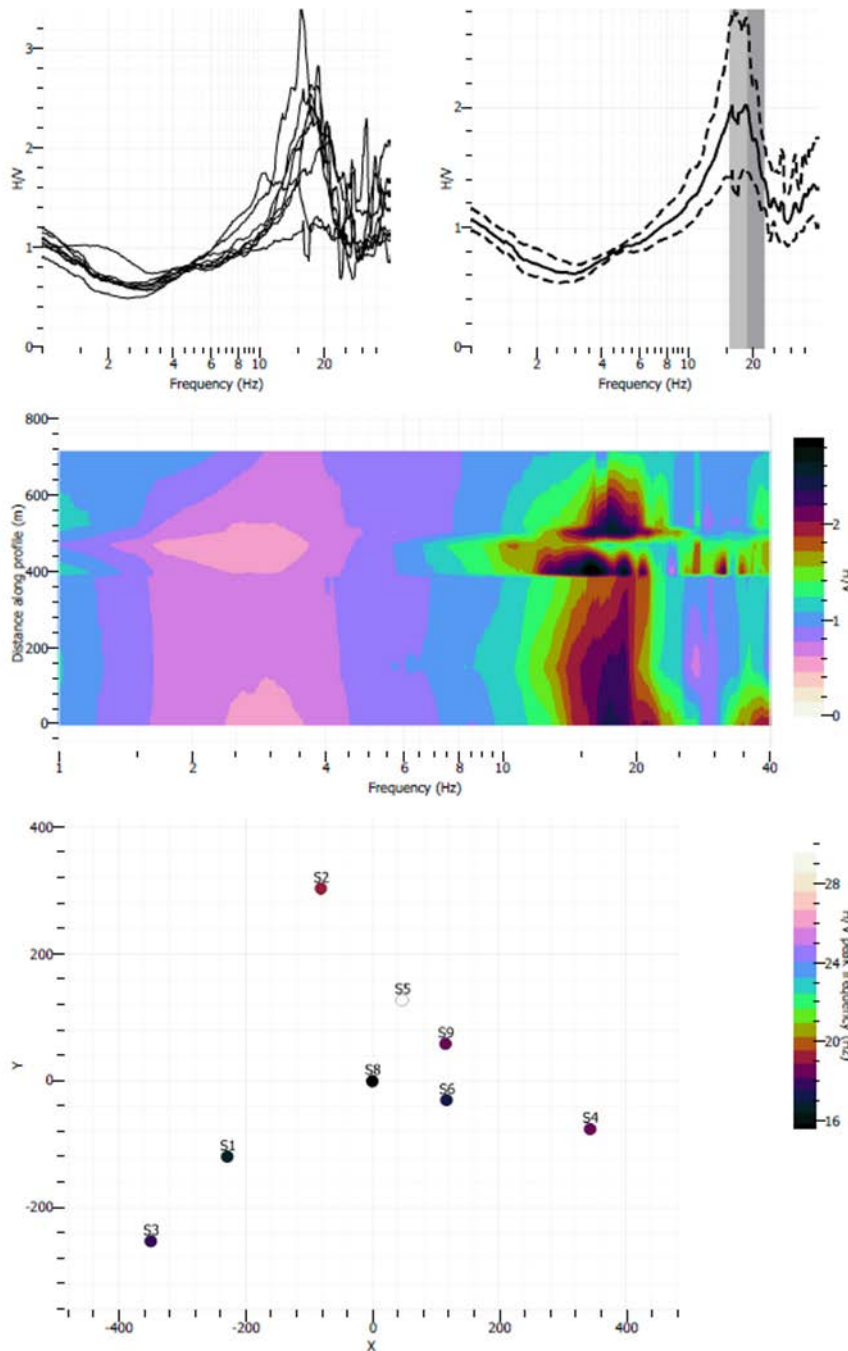
Figure 16: Summary report for the stations of the mini-array. All average curves (top left) and single curve showing the average of all individual curves, with amplitude and frequency standard deviations (top right). Frequency-distance graph with color-coded amplitude along a profile (middle) and map showing the distribution of the stations in a geographical system. On the map, each location is characterized by a color bubble, scaled to the peak frequency.

5.1.2 BUCHENHAIN DAS STATION

The design of the Buchenhain DAS station makes it possible to apply the same method as for a 3-component geophone with three measurement axes. The network of DAS SPs offers varying directivities, which enables selection of the components needed to calculate H/V spectral ratios. Thus, we select two surface SPs with orthogonal azimuths along the fiber, and select the shallowest borehole SP. For representativeness, we use here the data collected by DAS on January 22 over the same period

as the mini array data used previously in Section 5.1.1.The resulting H/V spectral ratio measurements are represented in Figure 17. It shows a consistent peak around 14 Hz, which is in agreement with the measurements obtained from the mini-array. However, we observe a low H/V ratio, below the typical value of 2. It suggests that the pic is an artifact rather than a signal related to the fundamental frequency.
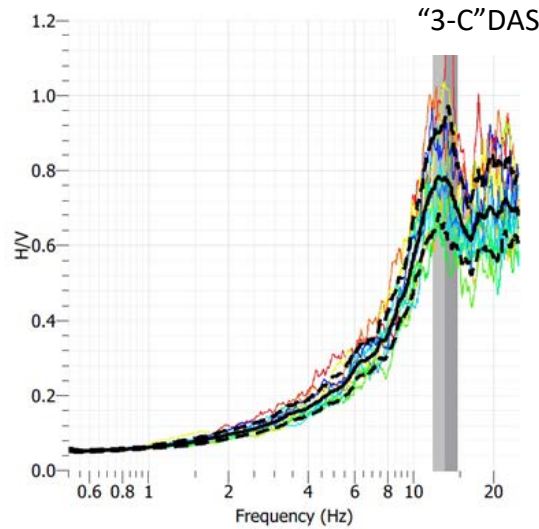
Figure 17: H/V spectral ratio computed with DAS data. The horizontal components are obtained from two SPs on the surface loop with orthogonal azimuths. The vertical component is obtained from the shallowest SP in the well. The H/V ratios (colored lines) are computed in consecutive windows defined along 30-minute-long DAS recordings. The black curve represents the averaged results over all colored individual H/V curves. The two dashed lines represent the H/V standard deviation. The grey area represents the averaged peak frequency and its standard deviation. The frequency value is at the limit between the dark grey and light grey areas.

5.1.3 INSIDE SURFACE NETWORK

We use the same procedure for 3C geophones of the "FORS", "FRIE", "BUCH" and "WBRU" stations as for the ones of the Siemens Park mini array. Figure 18 shows the results of the H/V spectral ratio analysis.

The station in Buchenhain yields a fundamental frequency f_0 that is comparable to the one evaluated using DAS data. The same applies to the station "FORS" and "WBRU", where f_0 is measured at 14 Hz. In the case of "FORS", we observe two peaks. They are not significant in view of the small value of the ratio. The slightly higher value measured at "FRIE" is in line with the measurements carried out on the Siemens Park mini array.
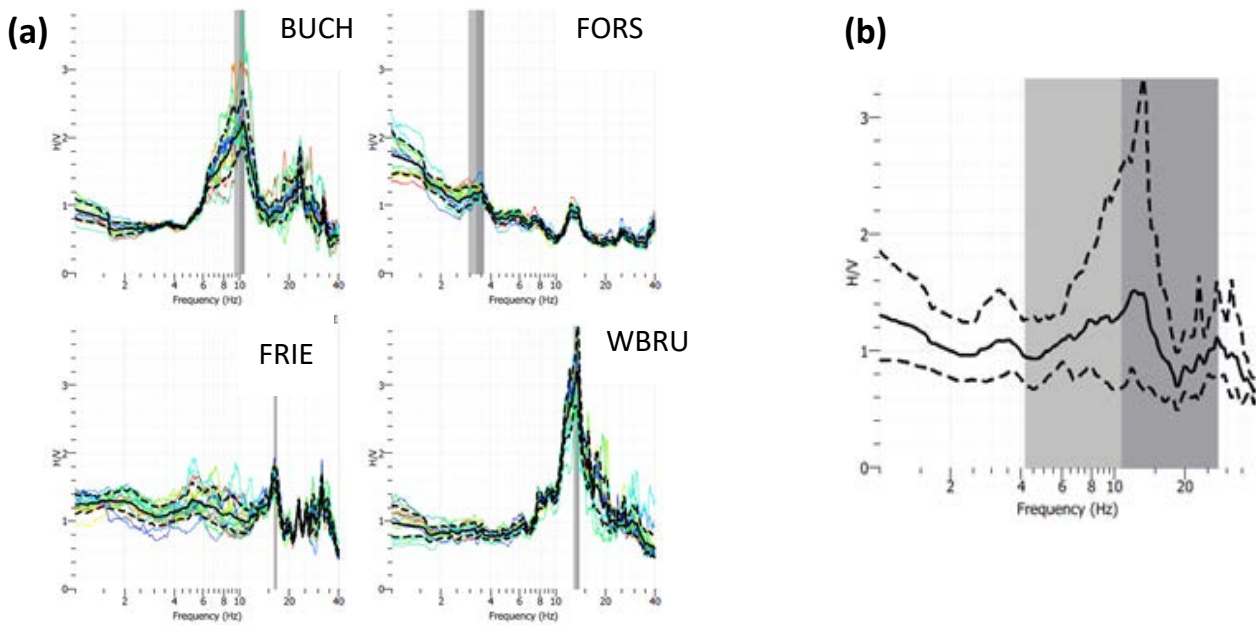
Figure 18: For each station of the seismometer network, panel (a) shows the H/V ratios computed in each successive window defined along the 30-minute-long recordings (colored curves). The black curve represents H/V geometrically averaged over all colored individual H/V curves. The two dashed lines represent the H/V standard deviation. The grey area represents the averaged peak frequency and its standard deviation. The frequency value is at the limit between the dark grey and light grey areas. The right diagram is a summary of all the results displaying the average and standard deviation.

5.2 VELOCITY MODEL DESCRIPTION

To broaden the scope of the site characterization analysis, we utilize the High-Resolution Frequency Wavenumber (HRFK) toolbox from GEOPSY package (Wathelet et al., 2020) to examine ambient noise vibrations (see Section 8.7), with the aim of characterizing the dispersion of surface waves and inverting a 1D velocity profiles.

5.2.1 MINI-ARRAY AND DISPERSION CURVES

We use data recorded on a Sunday before 4 am, to minimize the influence of anthropogenic noise on the ambient field vibrations. We apply the HRFK algorithm on all three components of the geophones within the mini-array.

Figure 19 shows the velocity versus frequency diagram obtained by applying the default Capon algorithm on the vertical components of all the mini-array geophones. The diagram shows, as a function of a log frequency scale, the velocity histograms (PDFs, as a color image) computed over the frequency bins used in the analysis, highlighting a clear Rayleigh wave fundamental mode in the 0.8 to 4 Hz frequency range. The mode is automatically picked from the maximum in the PDFs, yielding the velocity versus curve highlighted by black points. In addition, Figure 20 shows the associated power and azimuth histograms. The azimuth data reveal a consistent propagation direction for the Rayleigh wave in the frequency band of 0.8 to 4 Hz, with an azimuth of 220°.
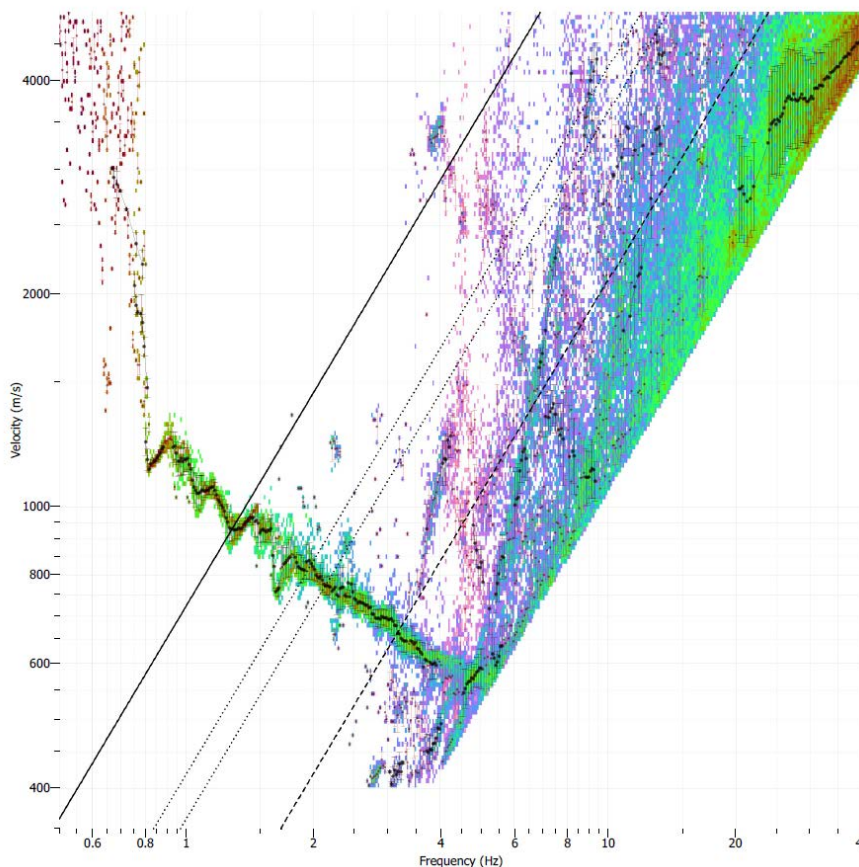
Figure 19: Diagram showing all the velocity histograms (PDFs) over the frequency bins used in the analysis. PDFs are computed over the successive windows where f-k analysis has been applied. They are displayed as a color image for a log frequency scaling. Here we use the default Capon algorithm on the vertical component of the sensors.
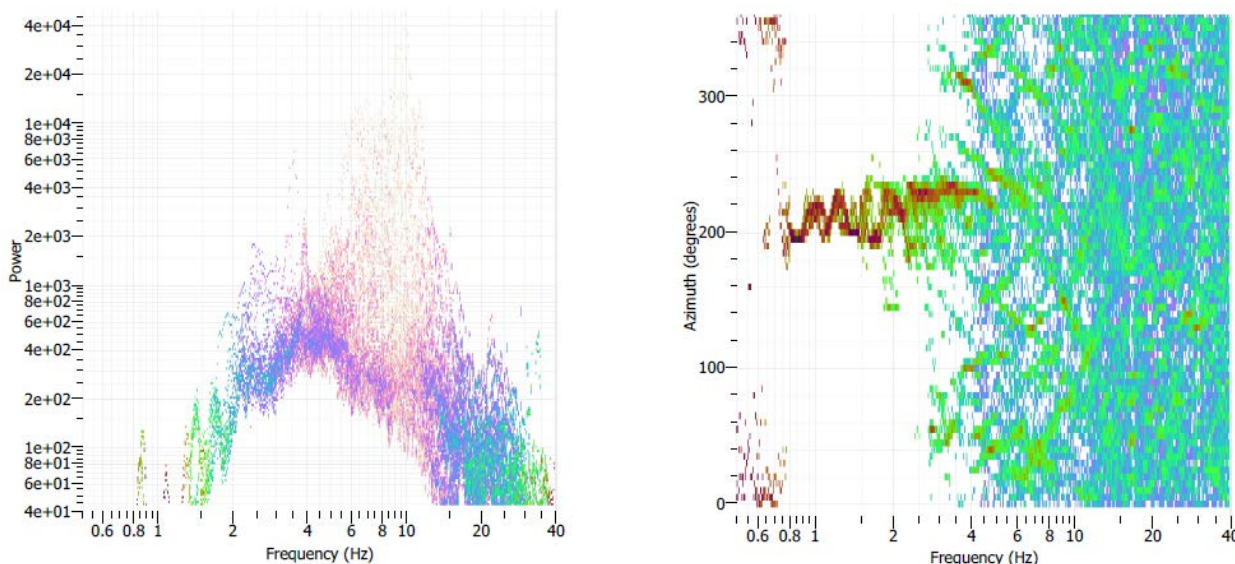
Figure 20: Power (left) and azimuth (right) histograms (PDFs) over the frequency bins used in the analysis. The PDFs are obtained from the measurements carried out in the successive windows where f-k analysis has been applied. The PDFs are displayed as a color image over a log frequency scale.

The Rayleigh dispersion curve obtained from the Capon analysis is used to invert a 1D-velocity profile using the GEOPSY package (see Figure 21). In Panel (a), the focus is on the dispersion curve, where the

black curves represent the data being inverted, and the colored curves depict the synthetic dispersion curves resulting from the inversion procedure. Panel (b) concentrates on the inverted subsurface properties, displaying synthetic P-wave (left) and S-wave (right) velocity profiles.

To evaluate the robustness of these measurements, the black dots represent data from sonic-logs conducted at the Schäftlarnstraße geothermal field. The black curve illustrates the velocity profile used to construct INSIDE velocity structure. In both panels, the color scale indicates the misfit between data and synthetics, with the lowest misfit shown in red and the highest misfit in blue.
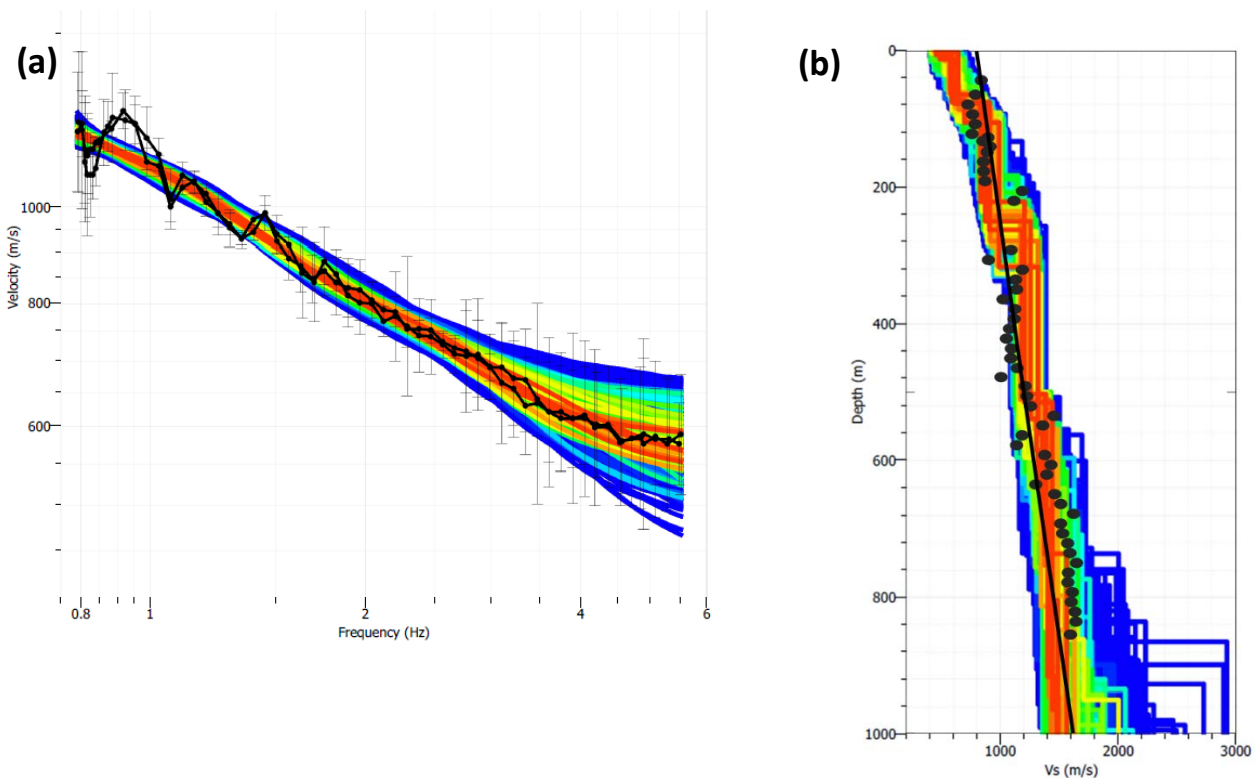
Figure 21: Results of inversion of the dispersion curves obtained by applying Capon analysis to the data recorded by the nine Siemens Park mini-array stations. Panel (a) focuses on the dispersion curve, with black curves showing the data being inverted and colored curves showing the results of the inversion procedure applied in GEOPSY (dinver software). Panel (b) focuses on the inverted subsurface properties. The colored curves show the synthetic shear-wave velocity profiles. To check the consistency of the inverted results, the black dots show sonic-log data from the Schäftlarnstraße geothermal field (in well TH3). The black curve shows the velocity profile used to build the velocity model. The color scale indicates the mismatch between data and synthesis (weakest mismatch in red, strongest mismatch in blue).

Figure 23 shows that the inversion of the Rayleigh dispersion curve produces a shear-wave (V$_S$) velocity profile that aligns with the data obtained from logging and the velocity structure. It effectively captures the higher gradient observed at shallow depths.

5.2.2 DAS IN WELL AND WADATI ANALYSIS
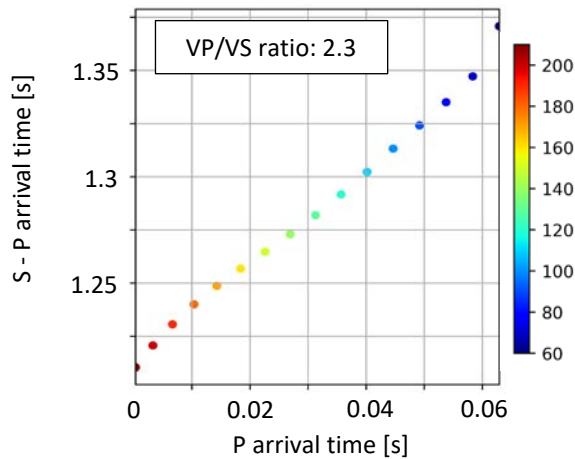
Figure 22: Results of the Wadati analysis performed on the DAS-data from the January 15, 2023 event (see Figure 27).

The DAS recordings made in the Buchenhain monitoring well allows the application of Wadati analysis. It allows deriving an average V_P/V_S ratio, providing the onset time of P- and S-waves along the vertical fiber. Figure 22 shows the results obtained with the recordings of the January 15 event, for which a significant signal strength and inter-channel coherence was observed on SPs along the monitoring well. We compute an average VP/VS ratio of 2.3 from these results (see Figure 22).

6 FINANCIAL ASPECTS

Finally, we compare the different types of stations installed, based on the associated design, installation and maintenance costs. A more detailed breakdown of costs is available in Appendix.

6.1 CONSTRUCTION COSTS

In the comparison illustrated Figure 21, we assess the construction costs associated with deploying monitoring stations, considering different instruments and configurations. The costs cover

- The purchase of sensors, recording devices and associated equipment (such as data loggers, storage devices, and routers for data transmission).
- The expenses related to enclosures and materials used for power supply, including batteries, AC/DC setups, and surge protection.
- The construction costs, which may include expenses related to excavation work or the drilling of wells in locations like Buchenhain.

Costs associated with the mini-array are difficult to estimate, as the sensors were rented to the Geophysical Institute KIT (GPI). However, we estimate below the cost for building the mini-array by supposing that the sensors (3-D Geophone PE-6/B by SENSOR Nederland) and the data loggers (DATA-CUBE3) have been purchased at this occasion.

Figure 21 shows that the costs associated with the DAS-station are significant, due to the construction of the FOC infrastructure (excavation work, preparation of monitoring well, etc.) and because of the price of the interrogation units. The costs associated with the DAS-station are ~8 times higher than the ones estimated for the mini-array, and ~20 times higher than for a surface seismometer station. These costs are largely driven (~40%) by the purchase price of a DAS system, which could however be shared by multiple sites and for multiple experiments on the longer term. The cost of drilling and excavation represents a smaller part of the overall costs (~20%). The purchase of the cable, which is the sensing-element and permanently installed, accounts for 5% of the total price.

The solution considered in the experiment in Schäftlarnstraße (temporary rental of a DAS system) is advantageous on a short term. The purchase costs are covered after 13 months of rental. The cable installed in the TH3 injection borehole was part of a collaboration between Geothermal Allianz Bavaria (GAB) and Technische Universität München (TUM). The associated costs are not assessed in this study.
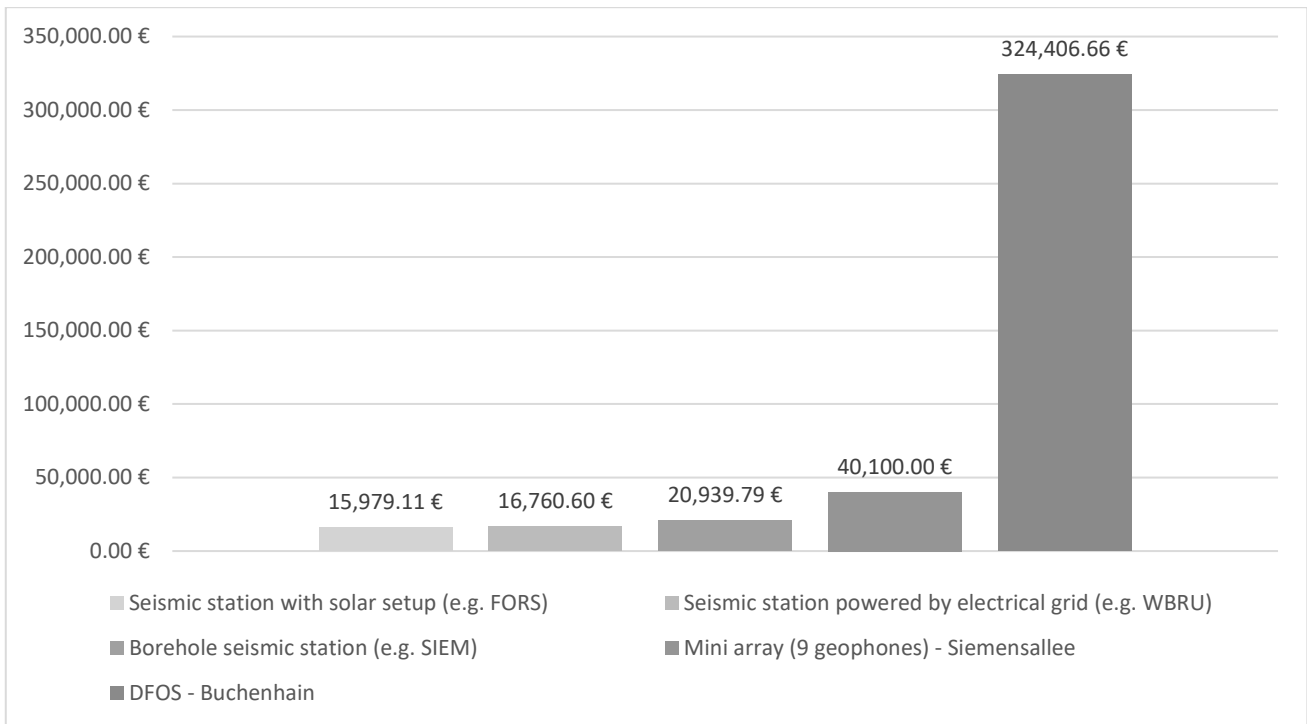
Figure 23: Comparison of construction costs for different measurement types and station geometries: surface / downhole seismometer stations, a mini-array of geophones and a Distributed Fiber Optic Sensing (DFOS) measurement station.

6.2 MAINTENANCE COSTS

Figure 24 compares the maintenance costs associated with the different monitoring stations and equipment. These maintenance costs cover the following components.

- Software updates: when available, e.g. for the fiber optic sensing interrogation units.
- Data transmission: when a router is used, which does not apply for the mini array, or for the fiber optic sensing station.
- Onsite fieldwork: for maintenance and data collection, considering trip(s) from Karlsruhe to Munich for two operators.
- Replacement parts: batteries (e.g. mini-array) and small supplies (like plastic covers).
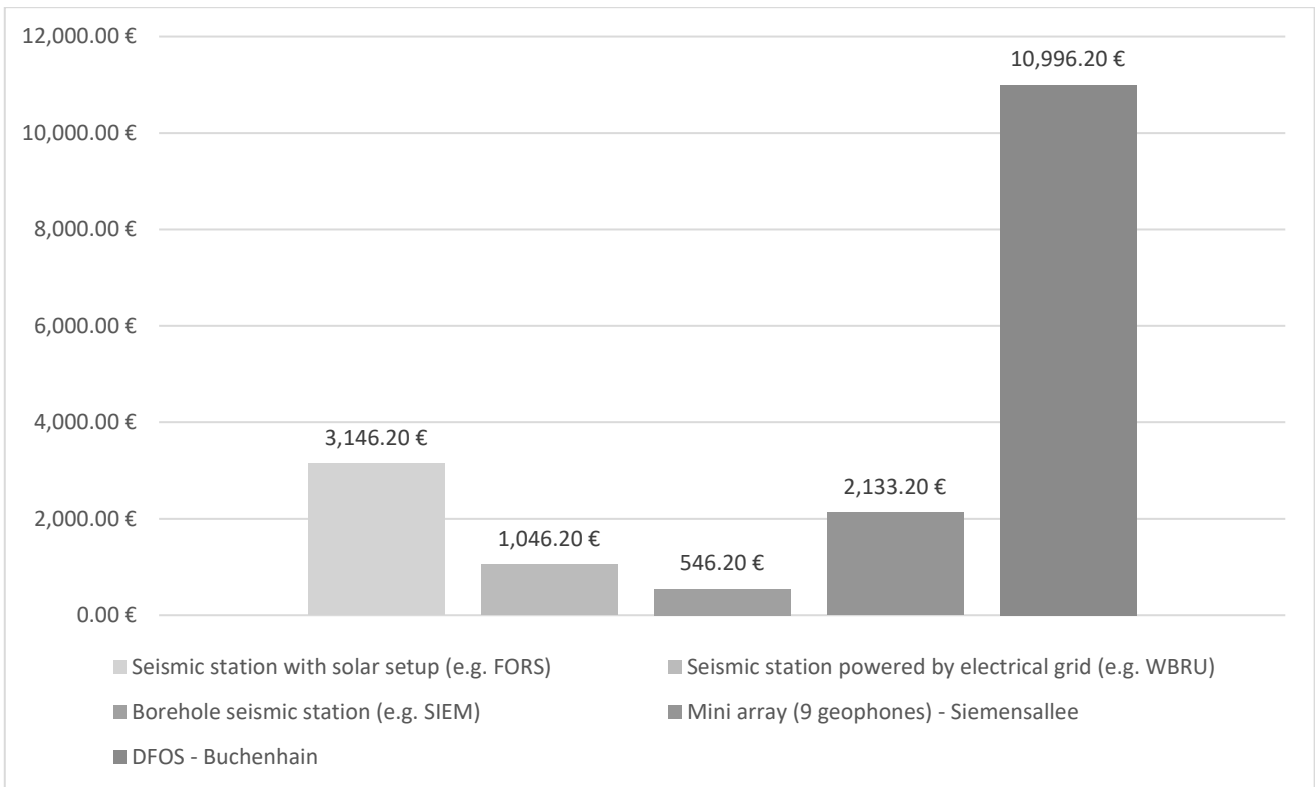
Figure 24: Comparison of maintenance costs for the different station types detailed in Figure 23.

As for construction costs, the DAS-station is the most expensive due to the service costs (upgrade and update) of the interrogators. Regarding the seismometer stations, relying on solar panels carries the risk of potential equipment replacement, such as batteries or solar panels. Use of the mini array comes at a price, due to the need to maintain the infrastructure (no automatic transmission of data) and replace batteries used for power supply.

6.3 CONCLUSIONS

The study shows the costs associated with the Buchenhain DAS-station are ~8 time higher than the ones estimated for the mini-array, and ~20 time higher than for a surface seismometer station. These costs are largely dominated (~40%) by the purchase price of a DAS interrogation unit and to a lesser extent by the price of drilling and excavation work (~20%). The purchase of the cable represents only 5% of the total price. However, the interoperability of the interrogator between different measurement sites is an important factor to consider: the firmly installed sensing element is the cable, which represents a minor part of the cost. The purchase of the Interrogation Unit can therefore be seen as a long-term investment. The temporary rental of a DAS interrogator is beneficial only in the short term, as the purchase cost is covered after 13 months of rental, from the experience conducted at Schäftlarnstraße.

The DAS station has the highest maintenance costs among the tested solutions. Maintenance costs are mainly due to the annual cost of maintaining and updating the interrogation unit. Data archiving and processing, e.g. via Microsoft Azure in the case of the Schäfltarnstraße experiment, entails additional costs which vary according to the data flow and the volumes to be retained. Downsampling can also be applied where relevant to reduce the quantity of data transmitted. For example, backing up all DAS datasets sampled at 500 Hz may be operationally irrelevant.

7 SUMMARY OF THE COSTS/BENEFITS ANALYSIS

The INSIDE project focuses on seismic monitoring in southern Munich, specifically the active Pullach and Schäftlarnstraße sites and the upcoming Baierbrunn project. The monitoring network used during the project includes four surface and one borehole station equipped with broadband geophones, a mini-array of geophones in the Siemens Park, a fiber optic sensing station in Buchenhain (with fibre optic cables installed in a 250-metre-deep monitoring well and near the surface), and a study was carried out in Schäftlarnstraße to investigate the seismic monitoring of the site using DAS from behind the injection well TH3. This report focusses on a comparison of the different seismic monitoring approaches considered in the INSIDE project and on the analysis of their associated pros and cons for seismic monitoring. This analysis comes in parallel of a description of the methodology developed to process data from the DAS station in Buchenhain and from the mini-array in Siemens-Park, and a description of the related monitoring results.

The project results underline the importance of the selection of measurement sites in relation to the monitoring target, and of precise station design (power supply, protection against the operating environment, coupling of the sensor…). These are operational constraints that apply to each measurement site, regardless of the method used. The contrast between the monitoring results for the different measurement methods should at best be analyzed independently of these practical aspects

The seismic signal detection capabilities are analyzed in view of the signal-to-noise ratios (SNRs) observed with the different instruments. This analysis is based on the catalogue of seismic events constituted during the project. Most of the observed seismic activity occurred near the Oberhaching and Unterhaching sites. The WBRU station (and to a lesser extent, BUCH) proved most beneficial for detecting events due to smaller source-to-receiver distances. A comparison of the absolute sensitivity of the stations, based on an analysis of SNRs relative to source-receiver distances, shows that FORS benefits from low noise levels. The results are consistent with noise measurements taken when the network was commissioned. Positioning the SIEM station in a borehole was of limited benefit, presumably due to poor coupling of the sensor to the ground, leading to lower sensitivity towards seismic signals. More effort would have been required for the SIEM station (e.g. cleaning the well, planning a better coupling with the addition of glass beads...).

The report then focuses specifically on the DAS station and the mini-array, detailing the seismic monitoring results and evaluating their benefits to seismic monitoring efforts compared to more conventional approaches. Applying beamforming to the mini-array recordings generally resulted in higher SNRs compared to using a bandpass filter on the closely installed SIEM borehole sensor. The back azimuth (BAZ) estimations from the mini-array are generally consistent with locations from the seismometer network. The results are hampered by operational issues and less reliance on station maintenance by KIT would have contributed to better performance of the mini-array.

The analysis of DAS data shows the potential of using the technology on cables installed in boreholes, either from a monitoring well or from behind the casing of a production well. The case study at the Schäftlarntraße geothermal site demonstrates an important contribution to the detection of seismic

event, allowing for increased sensitivity compared to surface measurements with minimal operational constraints. Additionally, DAS has proven useful for the estimation of seismic source characteristics at the two studied sites, Buchenhain and Schäftlarnstraße, and contributed to event localization. Our analyses show that it is nevertheless advisable to install a seismometer in parallel with a DAS measurement site, at least temporally, for the calibration of DAS measurements. For event localization, the Schäftlarnstraße experiment underscores a limitation of applying DAS technology to a single vertical well, due to its unidirectional sensitivity. The design of the Buchanhain station is particularly interesting for the estimation of wavefield directivity but would have benefited from a wider surface loop. In addition, the rich frequency content and the high spatio-temporal sampling of DAS data opens important perspectives in terms of data processing, which are still the subject of scientific development at present. Fiber optic cables can also facilitate the acquisition of various types of data, such as static temperature and strain profiles, expanding their monitoring capabilities beyond purely seismological applications.

The project's various experiments demonstrate the feasibility and advantages of using a hybrid network that combines different measurement techniques and locations. While financial considerations remain a barrier to the widespread adoption of DAS technology, it is advisable to equip future boreholes with cemented fiber optic cables, allowing a DAS interrogator to be connected temporarily during key monitoring periods (or permanently, if financially possible). The INSIDE project demonstrated, through experience and produced methodology, that the joint instrumentation of multiple borehole sites, potentially connected via surface telecommunication networks, in combination with a surface seismometer network, offers significant potential for monitoring geothermal reservoirs in urban environments. Apart from the densification of the model measurement network, the project outcomes also show that a well constrained speed model remains essential to avoid biases in the localization of the event, in particular due to the numerous measurement points introduced by the DAS detection technology.

Table 5: Summary of theoretical / expected and observed advantages and disadvantages for the three non-standard monitoring approaches evaluated in the frame of the INSIDE project

	Borehole seismometer SIEM	Mini-array in Siemens Park	DAS in Buchenhain	DAS in Schäftlarnstraße
Expected advantages	Measurements in well: higher distance to surface / noisy environment	Higher SNR with joint processing of 9 stations	Large array of sensing points, Higher SNR with joint processing of numerous measurement points (~450 m of cable, spacing of measurement points of 10 m)	Large array of sensing points, Higher SNR with joint processing of numerous measurement points (~700 m of cable, spacing of measurement points of 10 m)
		Possible study of wavefield directivity (back azimuth)	Measurements in well: higher distance to surface / noisy environment	Measurements in well: higher distance to surface / noisy environment, closer to reservoir

	Borehole seismometer SIEM	Mini-array in Siemens Park	DAS in Buchenhain	DAS in Schäftlarnstraße
			Cable directions cover multiple azimuths: possible study of wavefield directivity (back azimuth + incidence)	
Strength of seismic signals		35 events detected on seismometer network match the period of operation	41 events detected on seismometer network match the period of operation	Detection of 1 event that would have been unnoticed from the surface seismometers
		After beamforming, higher SNR than SIEM	30 events were further analyzed	2 events were further analysed
		18 events were further analyzed (SNR>3)		
Analysis of seismic wavefields		Back azimuths are consistent with the measurements from the seismometer network (12 out of 18 observed events)	For events adapted to the aperture of the array, demonstrated capabilities to study back-azimuth, incidence, moment magnitude, stress drop	Demonstrated capabilities to study back-azimuth, incidence, moment magnitude, stress drop
		Additional: Ambient wavefield processing; subsurface characterization using techniques like H/V spectral ratio or f-k processing of ambient seismic noise	Compatibility of the strain-rate data with ground motion acquired by seismometers for joint data processing	Compatibility of the strain-rate data with ground motion acquired by seismometers for joint data processing
			Limited resolution / sensitivity of the array for events observed near Oberhaching / Unterhaching (Array aperture)	DAS Unidirectional sensitivity limits event location capabilties from the single vertical DAS array in TH3
				Additional: infer properties from the surrounding medium from the study of the wavefield observed over the entire cable
Operational	Constraints related to sensor positioning and obtaining installation rights apply to all measuring stations, with more or less significant effects depending on the footprint of chosen measurement method / station design (surface area covered, number of sensors, flexibility of sensor arrangement)			

	Borehole seismometer SIEM	Mini-array in Siemens Park	DAS in Buchenhain	DAS in Schäftlarnstraße
	Coupling of sensors with formation is challenging from surface	With the proposed design, higher maintenance requirements than seismometer stations	The Buchenhain monitoring well additionally requires extensive planning, tendering and permitting, including decision on approval under water law	Efforts related to the installation of the fiber optic cable (done via GAB/TUM project) are not evaluated here
			Requirements in terms of data saving / processing infrastructure	Requirements in terms of data saving / processing infrastructure
Financial			The overall costs of the station are equivalent to ~8 mini array and ~20 surface seismometer stations	Rented DAS-System: purchase costs are covered after 13 months of rental
			Higher costs mainly due to the purchase/maintenance of the DAS-System	
			But the DAS System can be a long-term investment used on multiple sites	

\#

8 METHODS

8.1 BEAMFORMING

Beamforming is a signal processing technique used on the recordings of arrays of sensors to improve the signal-to-noise ratio and to localize the source of seismic events. Typically, beamforming allows evaluating the directionality of seismic waves.

Beamforming requires an array of sensors or receivers that receive concomitantly the signals from a particular source. Each sensor in the array introduces a time delay to the received signal. This delay is calculated based on the relative position of the sensor in the array, considering a direction of incoming signal and a slowness vector, generally characterized by two components (s_{XX} and s_{YY}) when the array is supposed to be included in an horizontal plane. The goal is to introduce delays in such a way that signals from the desired direction constructively interfere, while signals from other sources, such as incoherent background noise, interfere destructively. By adjusting the delays appropriately, the signals add up constructively and create a reinforced or "focused" signal. The optimal back azimuth and the local slowness vector can be evaluated.

The distinctive feature of Buchenhain's DAS station is its ability to combine DAS strain rate measurements from gauges oriented in different azimuths and inclinations. We use a 3D delay-and-sum beamforming algorithm (Johnson and Dudgeon, 1993) formulated in the time-domain to jointly analyze data from both the surface loops and the monitoring well and estimate ray parameters, including the back azimuth (BAZ, ϕ), incidence angle (INC, i), and apparent velocity of the wave field (v_{app}). The procedure assumes the propagation of a plane wave. For a set of candidate parameters, the algorithm uses Equation (1) to calculate the time delay τ between any SP j with coordinates (x_j, y_j, z_j) with respect to a reference location of coordinates (0, 0, 0), taken as the position of the wellhead. The effective, mean crustal velocity immediately below the array is noted v_c. Details on the formulation of the equation are provided e.g. by (Schweitzer et al., 2012)

$$\tau_j = \frac{-x_j \cdot \sin i \cdot \sin \phi - y_j \cdot \sin i \cdot \cos \phi + z_j \cdot \cos i}{v_c} \tag{1}$$

After applying time delays to each signal, the beamformed signal is computed by applying an average stack to the shifted traces. The beamforming intends to focus the direction to the hypocenter. The energy of the beamformed signal is estimated in consecutive overlapping data windows. Higher energy values indicate that the parameters focus the direction of maximum energy concentration, as constructive interference will result in higher amplitudes. The procedure is iterated for sets of candidate ray parameters.

In the context of array processing, wavenumber differences affect the array's ability to resolve and distinguish between different seismic waves. When an array detects seismic waves, it measures the apparent wavenumber, which can be used to infer the wave's direction and velocity. The resolution of an array in terms of wavenumber differences depends on several factors, including the aperture (size) of the array, the number of sensors, and their spatial arrangement, which are tied to its array transfer function (Johnson and Dudgeon, 1993; Rost and Thomas, 2002).

- The aperture of an array determines its resolution for small wavenumbers. A larger aperture allows the array to measure smaller wavenumbers, and the longest wavelength resolvable is roughly the same as the aperture. For wavelengths much larger than the aperture, the array behaves like a single station.
- More sensing points in an array improve its ability to filter out seismic energy with different slownesses, enhancing its wavenumber filtering quality.
- The spacing of seismometers influences the position of side lobes in the transfer function and the largest resolvable wavenumber. Smaller distances between seismometers allow the resolution of shorter wavelength seismic phases.
- The geometry affects the azimuthal dependence of resolution and side lobe positions.

Here, beamforming techniques are applied on the recordings of the Siemens Park mini-array (Section 8.2) and of the Buchenhain DAS station (Section 8.3 and 8.4). The aperture of both sensor arrays differs significantly: the mini-array spans over 600 m, while the SPs along the FOC near the surface extend across 35 m.

8.2 APPLICATION TO THE SIEMENS PARK MINI-ARRAY

We apply a delay-and-sum beamforming technique in the time domain. The algorithm is applied around the date/time of events triggered with the seismometer network (see Table 1) to the recordings of the nine geophones (see Figure 11) in various frequency bands.

The workflow is the following:

- We apply a Continuous Wavelet Transform (CWT) on each trace to evaluate the most prominent frequency in the time-frequency signature of the signal. We use a Morlet wavelet for the CWT.
- We apply a B.P. filter to the recordings of each station. For a robust assessment of the beam parameters for each of the events listed in Table 1, the delay and sum algorithm is run in different frequency bands, focusing on low frequencies ([1, 5] or [2, 10] Hz), or focusing on the frequency bands where the signal is most prominent.
- We apply the delay and sum algorithm in 2D for the set of stations operated at the time of the event. To account for the varying frequency content of the signals of the events from the catalogue, we explore different window lengths from 0.2 to .0.5 seconds. The beamforming results are evaluated for the frequency band / window where the highest beam power is observed.
- SNR is measured on the B.P. filtered traces, including on the merged beam trace.

Figure 25 illustrates a dataset from the Siemens Park mini-array for an event on September 25, 2022. The recordings from the mini-array for this particular event highlight a substantial SNR. The traces depict the measurements captured by the stations operational on that date (5 stations over 9).
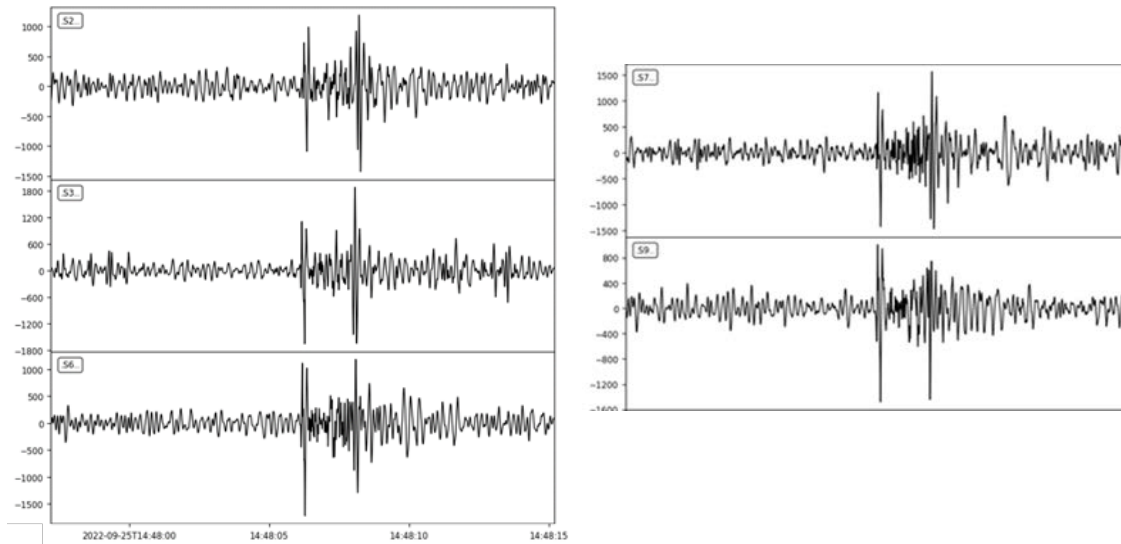
Figure 25: Example of dataset collected on the Siemens Park mini-array. The traces show the measurements of all stations that were operational on September 25, 2022. The recordings associated with the highlight a significant SNR Table 3.

Figure 26 illustrates the results obtained from the beamforming algorithm. Here it is applied to the recordings presented in Figure 25 after filtering the data in the [1, 5] Hz frequency band. The algorithm is applied along the signal to process in successive 0.3 s windows.
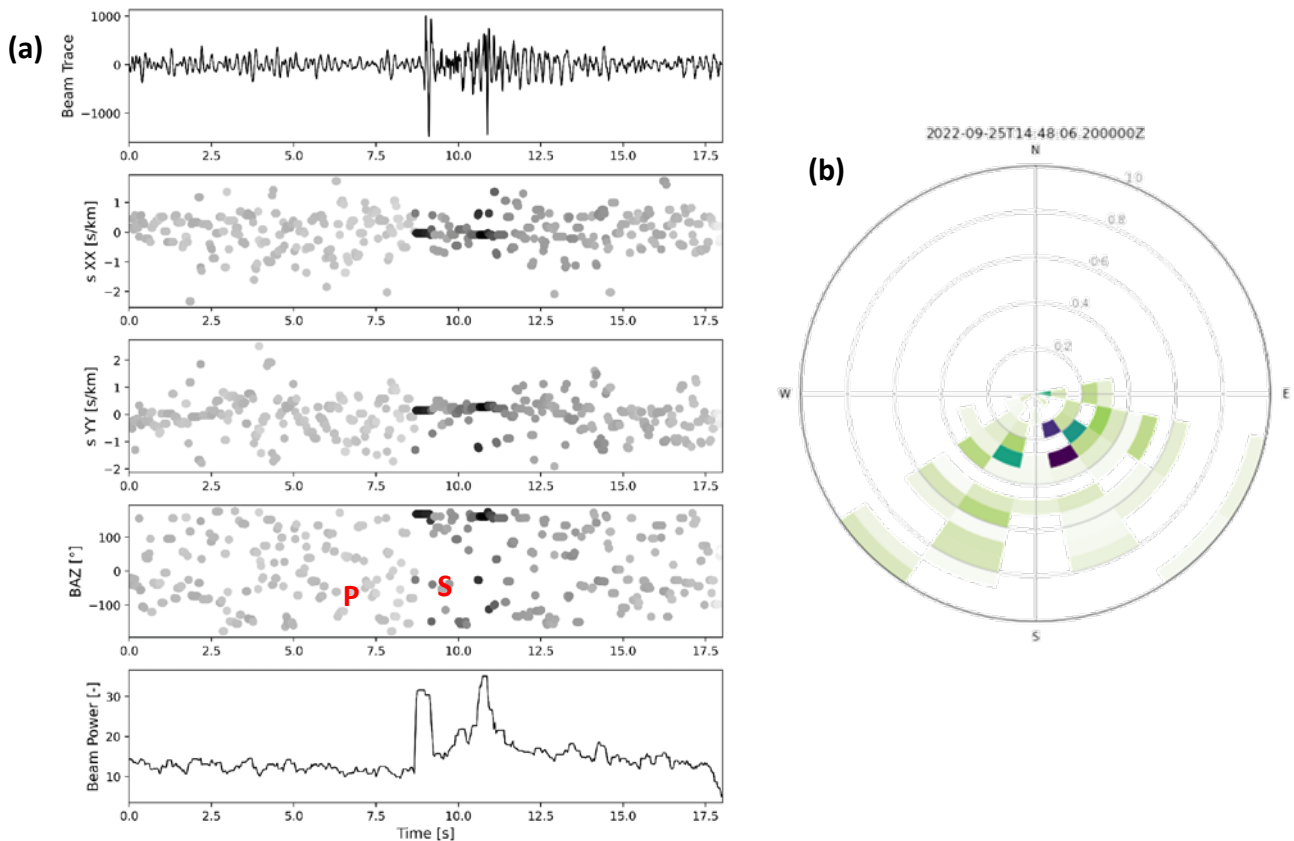
Figure 26: Example of beamforming results for the seismic event from September 25, 2022. Panel (a) shows, from top to bottom, the beam trace and associated beamforming parameters, i.e. the slowness components (s$_{XX}$ and s$_{YY}$) and the back azimuth (BAZ). The bottom trace shows the beam power. Panel (b) gives a polar representation of the results highlighting the inverted back-azimuth from the quarter with maximum beam power.

The beam trace presented in panel (a) features an increased SNR. The back azimuth to the seismic source is evaluated at maximum beam power, which shows significant peaks when the mini-array collects energy from the direct P and S-wave. We also evaluate the slowness components (s_{XX} and s_{YY}) associated to maximum beam power, which describe the wave field propagation. In panel (b), the results are displayed in a polar representation. It highlights the inverted back-azimuth from the quadrant with the maximum beam power.

8.3 APPLICATION TO THE BUCHENHAIN DAS STATION

At the Buchenhain DAS station, we are using the recording parameters listed in Appendix (Section 9.1). An example dataset is shown in Figure 27 for the event detected January 15, 2023, for which the DAS recordings show significant SNR (see Figure 6).
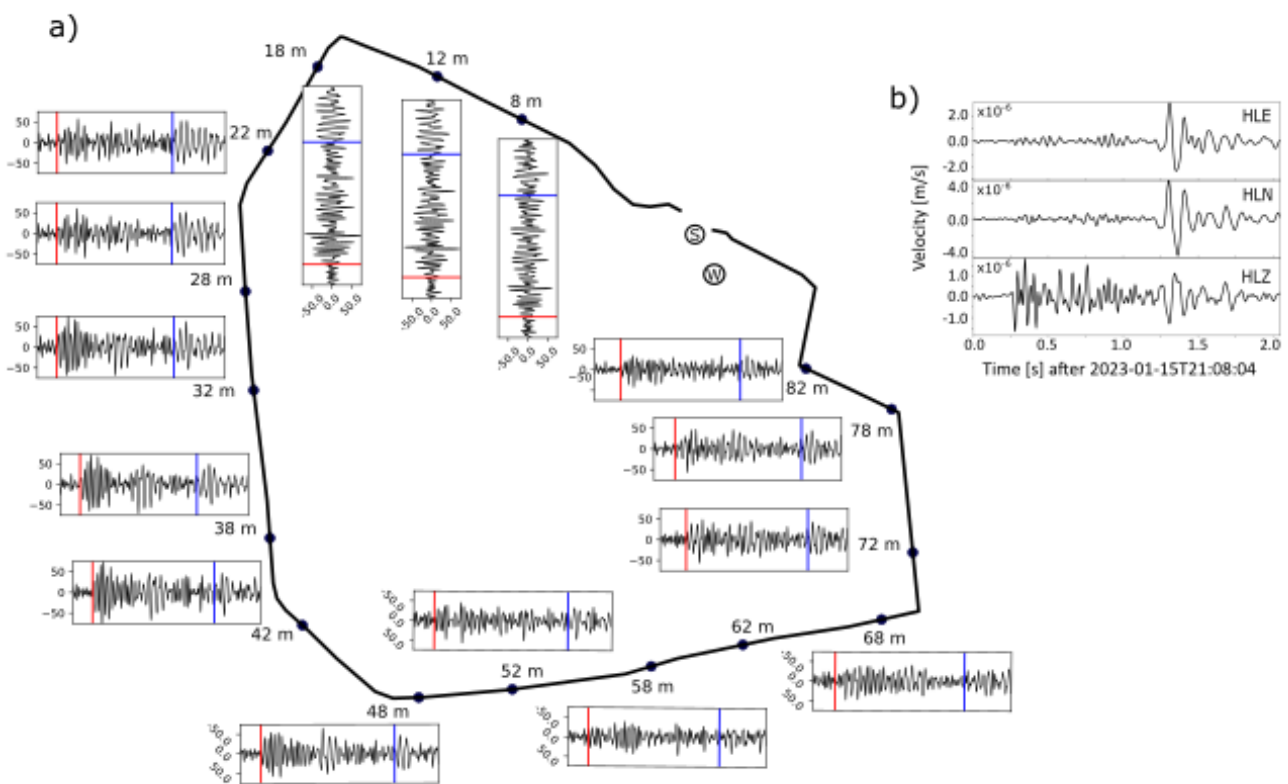
Figure 27: Example of dataset collected at the Buchenhain DAS station, on January 15, 2023. It is associated to an event for which the DAS recordings show significant SNR and a high frequency content (Table 3). The sensing points on the near-surface loops are shown in panel (a) with the arrival times measured for the first P- (red line) and S- (blue line) wave. Panel (b) shows the measurements associated with the BUCH seismometer, located in panel (a) with the circled S. The recordings are band pass filtered in the 5-50 Hz frequency band.
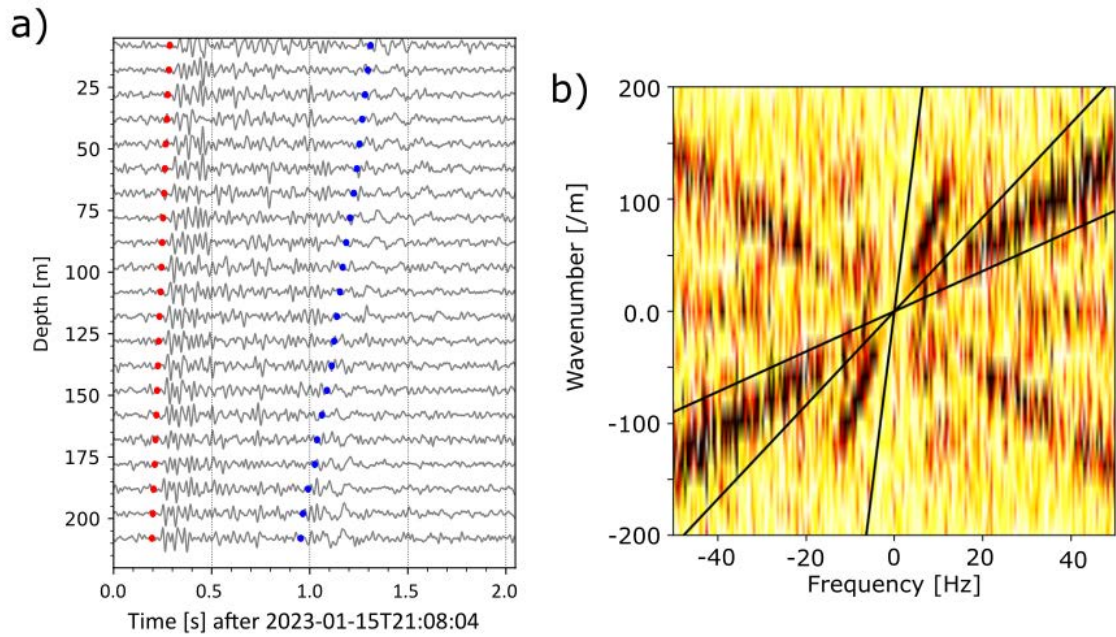
Figure 28: Example of dataset collected at the Buchenhain DAS station in the 250m deep monitoring well, on January 15, 2023. It includes the arrival times measured for the first P- (red star) and S- (blue star) wave. Panel (b) shows the dataset in the frequency wavenumber (f-k) domain. The solid lines correspond to apparent velocities of 3500, 1600 and 500 m/s
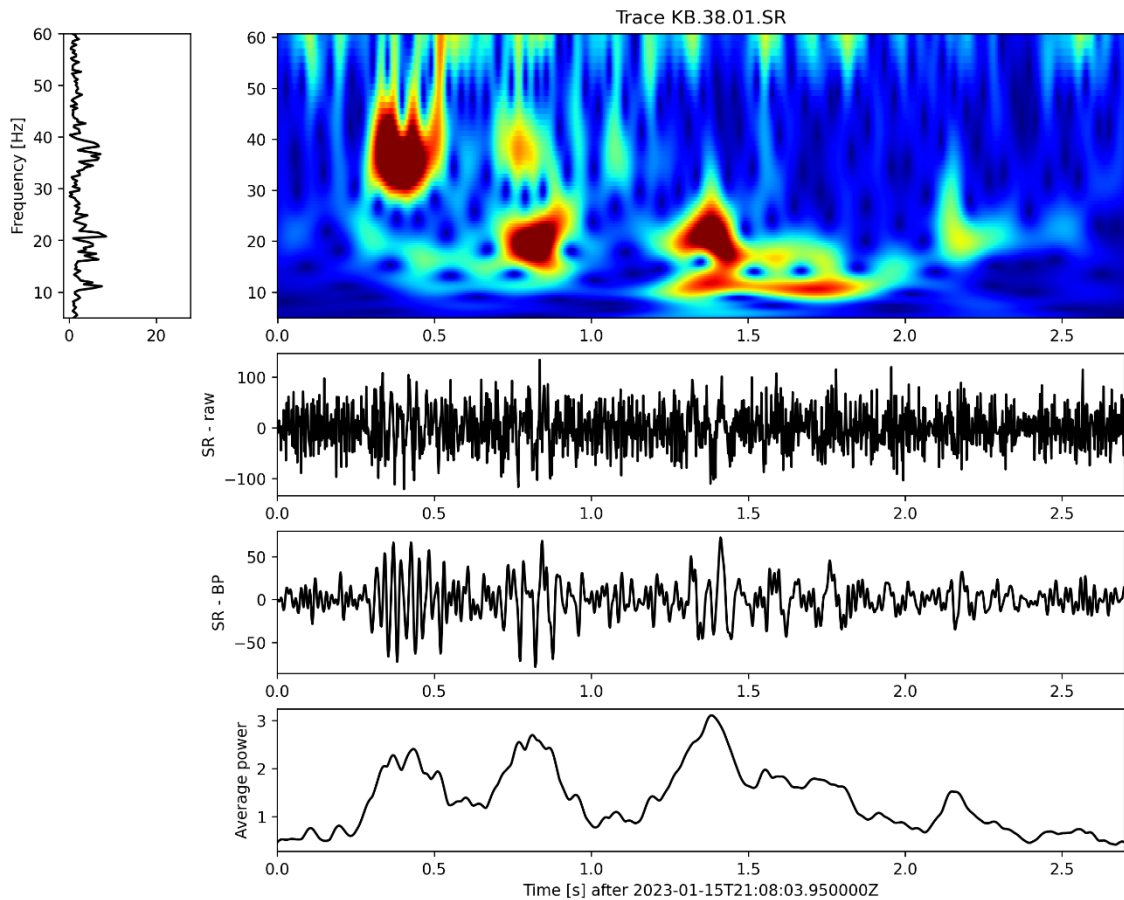
Figure 29: Time frequency representation, spectrum, average power and time series of the signal using a Continuous Wavelet Transformation (CWT) in the frequency domain, based on a Morlet Wavelet. The time-series is displayed without application of filter and after application of a band-pass filter in the 5-60 Hz frequency range. The calculation follows (Kristekova et al., 2006; Kristeková et al., 2009).

The processing steps applied to the DAS recordings for the estimation of ray parameters are the following:

- We apply a CWT (e.g. Figure 29) on each trace to evaluate the most prominent frequency in the time-frequency signature of the signal. We use a Morlet wavelet for the CWT.
- We apply a B.P. filter to the recordings of each station. For a robust assessment of the beam parameters for each of the events listed in Table 1, the delay and sum algorithm is run in different frequency bands, focusing on low frequencies ([1, 5] or [2, 10] Hz), or focusing on the frequency bands where the signal is most prominent.
- We apply a B.P. and f-k filter to the recordings of the monitoring well, by focusing on either the P- or the S-phase.
- We apply the delay and sum algorithm in 3D. To account for varying frequency content of the signal, we set the window length according to the main frequency of the signal of interest, taking 10 time the main period. The beamforming results are evaluated for the frequency band / window where the highest beam power is observed.
- SNR is measured on the B.P. filtered traces.

8.4 PROCESSING OF BOREHOLE DAS RECORDINGS

Additional processing is applied to the recordings of the monitoring well. The workflow includes the following steps:

- From the ray parameters estimated by beamforming, we shift and stack the traces, and measure the SNR on individual filtered traces and on the stacked trace.
- The inter-channels delays are also estimated in the temporal domain by cross-correlation of the traces. The processing results also in a correlation matrix covering all the DAS traces.
- For comparison, P-wave arrival times and delays are also measured using the HLZ channel of the BUCH seismometer, by cross-correlation of the two types of measurement types along the optical fiber.
- We estimate the P and S arrival times using the B.P. and f-k filtered dataset, focusing alternatively on the P-phase and on the S-phase. The traces are triggered using a STA/LTA algorithm to obtain a first estimate of the arrival time. The arrival time measured at the trace with highest SNR is refined to evaluate the onset time. The onset time is used to derive a template from the associated DAS recordings and the onset time is propagated across the dataset by cross-correlation.
- We convert the DAS SR traces to acceleration by application of the slant-stack method described previously.
- The converted DAS acceleration traces are used to evaluate the magnitude and stress drop by inversion, using a model for seismic source. We compare the DAS recordings at depth to the recordings of the vertical (HLZ) channel of the BUCH seismometer, located on the surface.

An example dataset is shown in Figure 27 for the event detected January 15, 2023, for which the DAS recordings show significant SNR (see Figure 6). In addition to the standard band-pass (B.P.) filtering applied on other measurement types / configurations, the long vertical (unidirectional) array of SPs allows the application of filtering techniques in the frequency-wavenumber (f-k) domain. These methods enable to focus on the wave field propagating from bottom to top of the FOC and / or on specific phases. The procedure is illustrated in Figure 27 where panel (a) shows the wave field after application of a B.P. and an f-k filter. Panel (b) shows the unfiltered dataset in the f-k domain. The f-k filtering approach consists in eliminating the energy of waves propagating downwards (upper-right and lower-left quarters) in the f-k domain. For the automatic picking of P- and S- waves, the f-k filtering can be more selective, allowing it to concentrate specifically on either the upward-propagating P-phase or S-phase. For that purpose, we retain only the energy in the narrow bands delimited by the black lines in panel (b).

Downhole DAS recordings are also used to resolve seismic source parameters such as the scalar moment tensor (M_0), the moment magnitude (M_W) and the stress drop (ΔS). The approach is based on fitting the observations with a model describing the amplitude spectrum of the seismic signal at a given distance of the seismic source (Anderson and Hough, 1984). It requires previous knowledge of the location of the seismic source, and the conversion of the DAS SR data to acceleration. The conversion is carried out by dividing the SR values by the apparent slowness of the wave field. For a more robust conversion, we propose to evaluate a time series of slowness values over the seismic signal, rather than using a fixed value. This is achieved by the slant-stack processing illustrated in Figure 30. DAS traces are isolated around the trace to be converted. Here, this coherence domain extends over 100 m. The slant-stack consists in shifting the traces within this coherence domain and estimating the coherence of the shifted traces. For each timestamp over the seismic signal, several slowness values are tested, resulting in the semblance matrix shown in panel (a). The slowness time series used for the conversion of the trace at depth is obtained by maximizing the matrix over time.
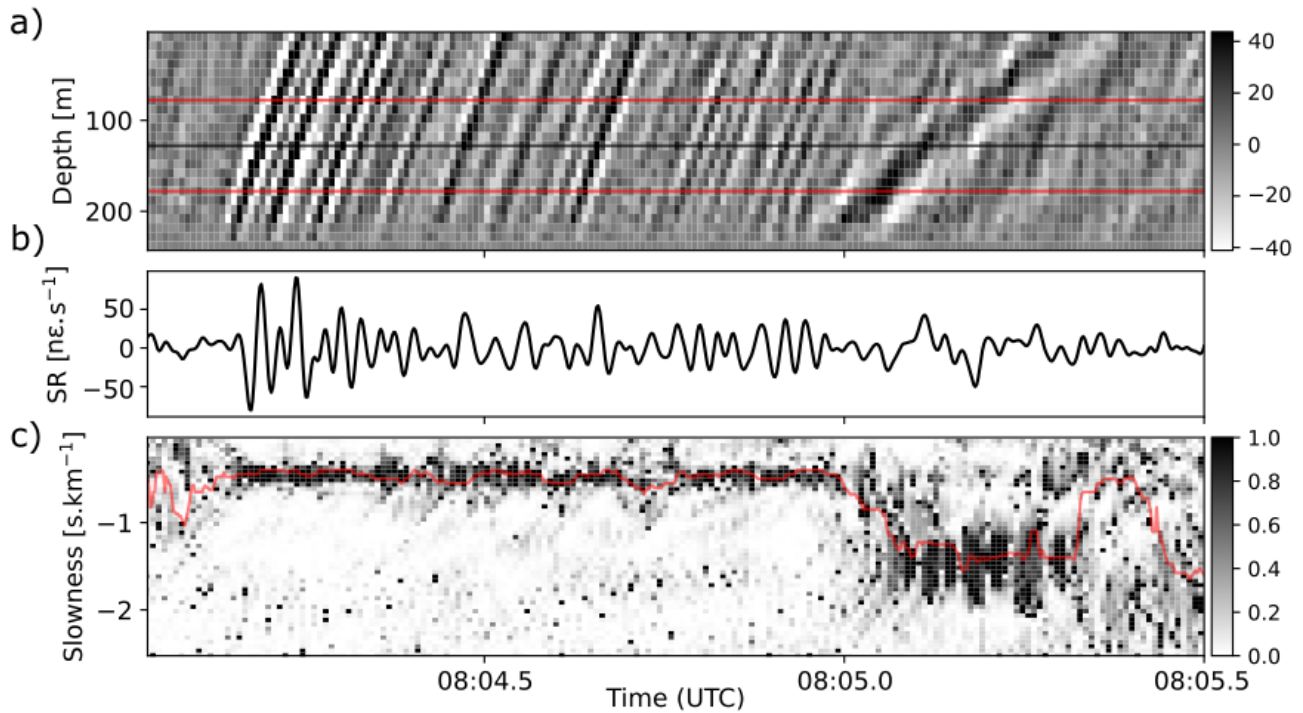
Figure 30: Conversion of DAS data from SPs in the well to acceleration and comparison with measurements from the BUCH seismometer. Panel (a) shows the SR data chunk (delimited by red lines) used for the conversion, tacking the example of the conversion of the trace located at 120 m depth (black line). Panel (b) shows the SR waveform considered for conversion. The semblance matrix for the queried trace within the data chunk is shown in panel (c). It includes the slowness time-series used for conversion as a red line.

Figure 31 compares the converted trace (black) to the recordings of the vertical component of the BUCH seismometer, showing the consistency between the two traces in both phase and amplitude.
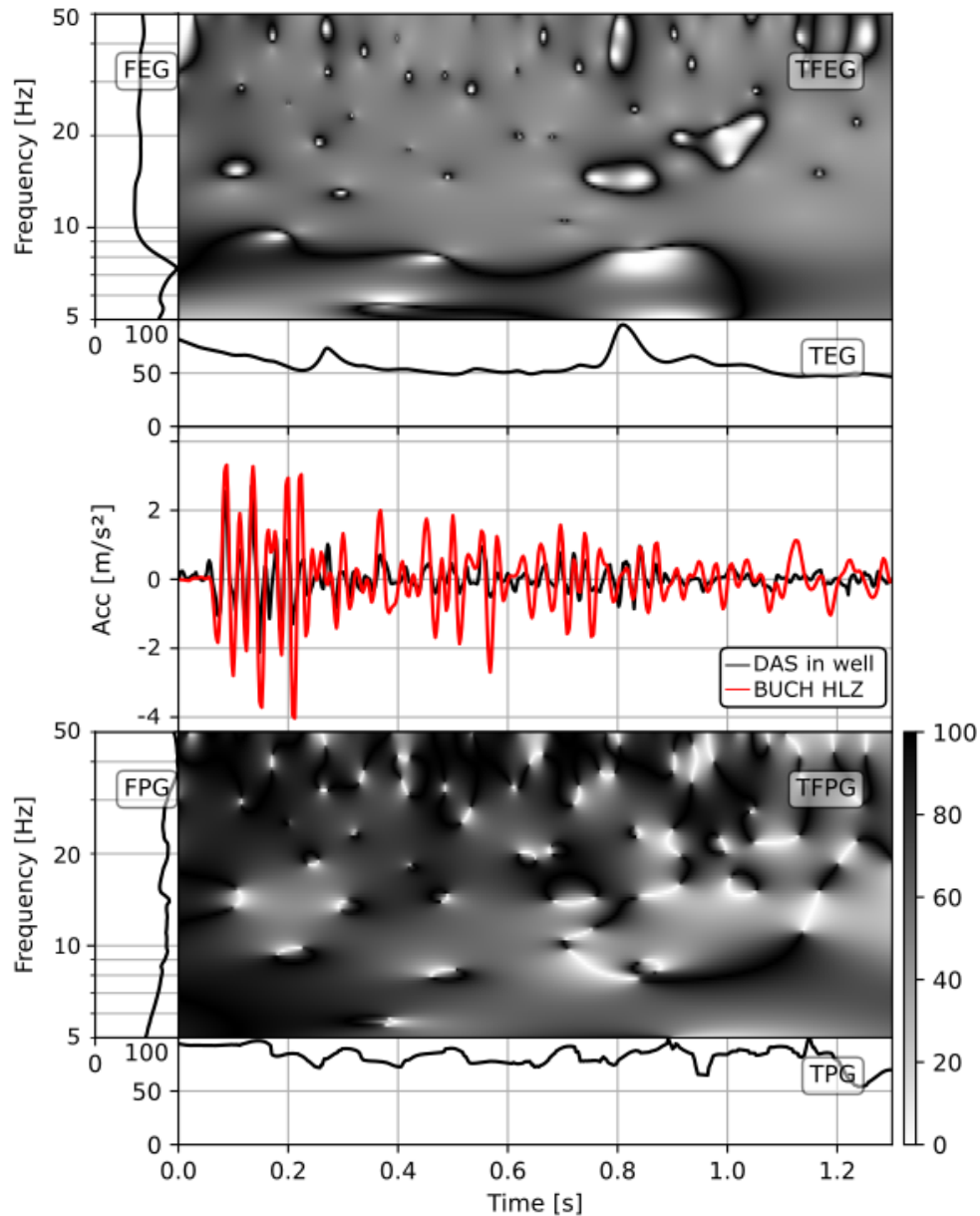
Figure 31: Time-frequency comparison between the vertical components BUCH HLZ and the converted DAS waveform for the SP at a depth of 20 m in the monitoring well, the middle rows compare the considered channel of the BUCH station (black curve) and the DAS waveform (red curve) once converted to acceleration. Top rows show the normalized goodness-of-fit (GOF) of the waveform envelopes in the time-frequency domain (TFEG) and its average over frequencies (FEG) and over time (TEG). The content of the bottom rows is similar to the top rows, but the GOF is calculated on the waveform phases (TFPG, FPG, TPG).

After conversion, the Fourier amplitude spectrum of acceleration is computed and compared to modelled spectra, with varying parameters. The fit is estimated between observed and modelled spectra. Values for scalar moment M_0, moment magnitude M_W and stress drop ΔS are derived from the best-fitting spectrum. The results for the January 15 events are shown in Figure 32, where they are compared to the measurements obtained from the seismometer network. The procedure is repeated for every DAS sensing point. Hence, we compare all M_0 and M_W values obtained from each DAS SP to the estimates derived from the seismometer network using a ratio. The figure shows the consistency between both datasets, with ratio values close to 1.
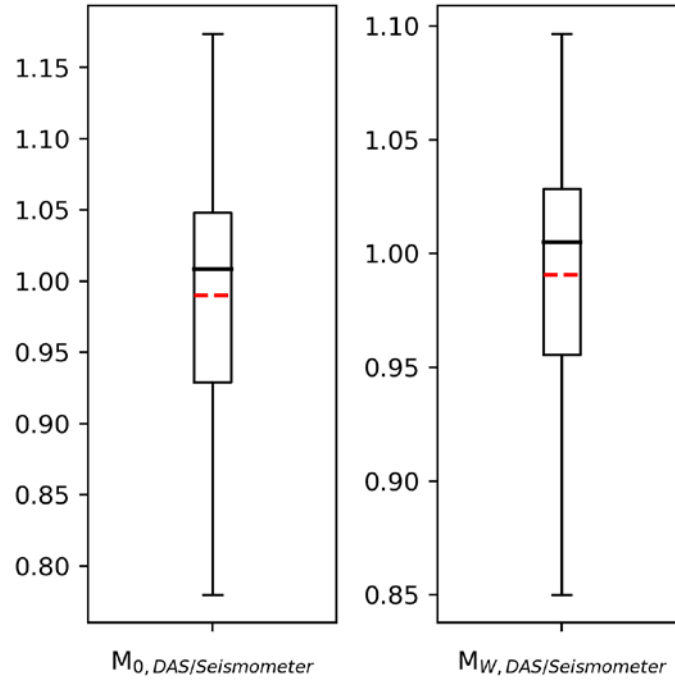
Figure 32: Results of the seismic source inversion using DAS sensing points located in the 250 m deep Buchenhain well. Panel (a) is an example of inversion showing the observed amplitude spectrum (red curve) along with the best fitting synthetic one (black curve). Panel (b) illustrates, for the inversion presented in panel (a), the selection of the model parameters, i.e. the corner frequency f0 and the plateau amplitude Ω0. In panels (c) and (d), a comparison is presented between the scalar moment (M0) and moment magnitude (MW) values obtained from each DAS SP and the estimates derived from the Buchenhain seismometer. The boxplot illustrates the distribution of ratios between DAS- and seismometer-estimated values for both seismic source parameters. The green line represents the mean, the orange line corresponds to the median, and the whiskers extend from the lowest to the maximum value in the dataset.

Consequently, the DAS station makes it possible to resolve the directionality of the seismic waves unambiguously (back azimuth and incidence) and estimate the associated magnitude, which is exemplified in the following.

8.5 CONVERSION OF DATA TYPES

Considering the propagation of a non-dispersive plane wave at location $\vec{r}$ and time t with a slowness-vector $\vec{s}$, the particle displacement $\vec{u}$ can be expressed as a function of $\vec{U}$, its polarization and f, the shape of the wave or d'Alembert's solution to the wave equation:

$$\vec{u}(\vec{r},t) = \vec{U} f(\vec{s}\vec{r} - \vec{t}) \tag{S1}$$

Then, linear strain-rate $SR(\vec{r},t)$ in the any direction x, defined by its azimuth φ_x is:

$$SR(\vec{r},t) = \frac{d}{dt}\frac{d}{dx} u_x(\vec{r},t) = \frac{d}{dt} U_x s_x f'(\vec{s}\vec{r} - \vec{t}) = U_x^2 s_x f''(\vec{s}\vec{r} - \vec{t}) \tag{S2}$$

Likewise the x-component of particle acceleration $a_x(\vec{r},t)$ is:

$$a_x(\vec{r},t) = \frac{d^2}{dt^2} u_x(\vec{r},t) = U_x^2 f''(\vec{s}\vec{r} - \vec{t}) \tag{S3}$$

The scaling relation between strain-rate and acceleration is therefore given by:

$$SR(\vec{r},t) = s_x \cdot a_x(\vec{r},t) \text{, simplified as } SR(t) = s_x \cdot a_x(t) \tag{S4}$$

8.6 H/V SPECTRAL ANALYSIS

The technique originally proposed by (Nogoshi and Igarashi, 1971), and widespread by (Nakamura, 2000), consists in estimating the ratio between the Fourier amplitude spectra of the horizontal (H) to vertical (V) components of the ambient noise vibrations recorded at one single station. The H/V spectral ratio curve represents how ground motion amplitudes vary with frequency for both horizontal and vertical motions. The fundamental frequency f_0 of the site is estimated from the H/V spectral ratio curve. It is associated with a peak in the H/V ratio curve, which corresponds to the dominant frequency at which the site amplifies ground motion.

We use the H/V module of the GEOPSY software package (Wathelet et al., 2020) for the processing of the array vibration recordings. The analysis is carried out in successive windows. The duration of the windows is frequency dependent and fixed at 50 times the central period of the studied frequency bin. In agreement with the SESAME user guidelines (Bard et al., 2008), we use the anti-triggering algorithm available in the GEOPSY suit on raw and filtered signals to select the most stationary windows.

The H/V spectral ratio method provides valuable information for earthquake hazard assessment, site-specific seismic design, and the selection of appropriate building codes and construction practices. In case of high impedance contrast between soft filling and deeper layers and under the 1D assumption, f_0 is identified as the resonance frequency. This information can be used to assess the site's susceptibility to seismic amplification. Sites with lower resonance frequencies tend to amplify longer-period seismic waves, which can be more damaging to certain types of structures. High resonance frequencies may indicate a site that amplifies higher-frequency waves. Under the same assumptions, the H/V peak frequency can be associated to H, the thickness of the soft layer, and V_S, the average shear-wave velocity in the soft layer: $f_0 = V_S / 4H$.

8.7 AMBIENT SEISMIC WAVEFIELDS AND DISPERSION CURVES

Ambient seismic wavefield recordings from large arrays can also be used to study the dispersive behavior of surface waves extracted from the ambient noise using frequency wavenumber techniques.

We use the high-resolution frequency wavenumber (hrfk) Toolbox from the GEOPSY package (Wathelet et al., 2020) to analyze ambient noise vibrations. The algorithm follows (Capon, 1969) that introduced a generalized beamforming algorithm resulting in an auto-adaptive spatial weighting scheme for analysis of narrowband stationary signals. As for the H/V method, the approach consists in analyzing the data in successive time-windows focusing on narrow frequency bands. Here, we define 500 frequency bands from 0.5 to 40 Hz. We scale the window length to the central frequency of each frequency band to be processed. We consider successive windows of 50 T, with T the central period of the band.

This analysis is equivalent to an iterative frequency wavenumber analysis carried out in windowed datasets. The statistical representation of the results can highlight the dispersive nature of surface waves in ambient noise recordings. Dispersion curves are graphical representations of the relationship between the phase velocity (velocity at which a particular frequency component of seismic waves propagates) and frequency. Dispersion occurs because different frequencies travel at different speeds through the Earth's materials. The dispersion curves obtained from seismic arrays and ambient vibration recordings can be used to infer subsurface properties (dispersion curve inversion). This inversion process typically involves modeling the subsurface structure and material properties to match the observed dispersion curves. For the inversion, we use here the inversion software available from GEOPSY.

9 APPENDIX

9.1 DAS RECORDING PARAMETERS

BlockRate = 1000 ms

FiberLength = 750 m

Hostname': b'fa1-20050034',

PulseRateFreq = 10000000 Hz

PulseWidth = 3 m

SamplingRate = 250 MHz

SamplingRes = 40 cm

AmpliPower = 28 dB

DerivationTime = 2.0 ms

GaugeLength = 20.0 m

9.2 ESTIMATION OF INSTALLATION AND MAINTENANCE COSTS

Table 6: Breakdown of costs for the installation and maintenance of the various seismic monitoring methods set up as part of the INSIDE project

Seismic station with solar setup (e.g. FORS)

FIXED COSTS	[€] (No VAT)
COSTS FOR INSTALLATION	
Solar panels, electrical equipment (batterie, AC/DC, converter), sensor housing, cabinet and frame, router	2,122.61 €
COSTS FOR SENSING MATERIAL	
Trillium Compact Vault 20s	6,919.85 €
Centaur 3CH	6,586.65 €
Transmission cable	350.00 €
TOTAL	15,979.11 €

YEARLY MAINTENANCE	[€] (No VAT)
Associated trips to Munich	
x 2 / year	1,000.00 €
Costs for parts replacement	1,500.00 €
Sim card subscription	46.20 €
Site rental	600.00 €
TOTAL	3,146.20 €

Seismic station powered by electrical grid (e.g. WBRU)

FIXED COSTS	[€] (No VAT)
COSTS FOR INSTALLATION	
Connection to electrical grid	3,000.00 €
Electrical equipment (batterie, AC/DC), sensor housing, cabinet, router	2,060.60 €
COSTS FOR SENSING MATERIAL	
Trillium Compact Vault 20s	5,815.00 €
Centaur 3CH	5,535.00 €
Transmission cable	350.00 €
TOTAL	16,760.60 €

YEARLY MAINTENANCE	[€] (No VAT)
Associated trips to Munich: x 1 / year	500.00 €
Costs for parts replacement	-
Sim card subscription	46.20 €
Site rental	500.00 €
TOTAL	1,046.20 €

Borehole seismic station (e.g. SIEM)

FIXED COSTS	[€] (No VAT)
COSTS FOR INSTALLATION (cabinet available)	
Electrical equipment (batterie, AC/DC), sensor housing, cabinet, router	1,054.79 €
COSTS FOR SENSING MATERIAL	
Trillium Compact PH 120s	6,565.00 €
Centaur 6CH	6,660.00 €
Lifting assembly	130.00 €
Transmission cable	6,530.00 €
TOTAL	20,939.79 €

YEARLY MAINTENANCE	[€] (No VAT)
Associated trips to Munich	
x 1 / year	500.00 €
Costs for parts replacement	-
Sim card subscription	46.20 €
Site rental	???
TOTAL	546.20 €

Fiber Optic Sensing - Buchenhain

FIXED COSTS	[€] (No VAT)
COSTS FOR INSTALLATION	
Station construction (permitting, excavation and drilling, constrution of the station)	55,584.01 €
Electrical equipment (batterie, AC/DC, converter), sensor housing, cabinet and parts, router and other IT resources	4,801.65 €
COSTS FOR SENSING MATERIAL	
CABLES, DAS and DTSS	16,926.00 €
FEBUS G1R	66,725.00 €
FEBUS A1R	134,850.00 €
FEBUS on site services and shipment	17,780.00 €
Data storage 20TB	22,400.00 €
Rack system 19'' with equipment + UPS	5,340.01 €
TOTAL	324,406.66 €

YEARLY MAINTENANCE	[€] (No VAT)
Associated trips to Munich	
x 3 / year	1,500.00 €
Costs for parts replacement	100.00 €
Sim card subscription	46.20 €
Site rental	1,500.00 €
Software Update A1/G1	7,850.00 €
TOTAL	10,996.20 €

Mini array (9 geophones) – Siemens Park

FIXED COSTS	[€] (No VAT)
COST FOR STATION	
Permitting	-
Batteries	see maintenance
Parts (plastic covers, cables)	50.00 €
COST FOR SENSING MATERIAL	
Geophones (x9)	4,050.00 €
Data CUBES (x8)	36,000.00 €
TOTAL	40,100.00 €

YEARLY MAINTENANCE	[€] (No VAT)
Associated trips to Munich x 3 / year	1,500.00 €
Costs for parts replacement	50.00 €
Batteries	583.20 €
Sim card subscription	-
Site rental	-
TOTAL	2,133.20 €

DAS Rental

FEBUS A1-R: Distributed Acoustic Sensing System Site rental (per month)	10,472.00 €

10 BIBLIOGRAPHY

Anderson, J.G., Hough, S.E., 1984. A model for the shape of the fourier amplitude spectrum of acceleration at high frequencies. Bulletin of the Seismological Society of America 74, 1969–1993. https://doi.org/10.1785/BSSA0740051969

Azzola, J., Gaucher, E., 2024. Seismic Monitoring of a Deep Geothermal Field in Munich (Germany) Using Borehole Distributed Acoustic Sensing. Sensors 24, 3061. https://doi.org/10.3390/s24103061

Azzola, J., Thiemann, K., Gaucher, E., 2023. Integration of distributed acoustic sensing for real-time seismic monitoring of a geothermal field. Geotherm Energy 11, 30. https://doi.org/10.1186/s40517-023-00272-4

Bard, P.-Y., Acerra, C., Aguacil, G., Anastasiadis, A., Atakan, K., Azzara, R., Basili, R., Bertrand, E., Bettig, B., Blarel, F., Bonnefoy-Claudet, S., Paola, B., Borges, A., Sørensen, M., Bourjot, L., Cadet, H., Cara, F., Caserta, A., Chatelain, J.-L., Zacharopoulos, S., 2008. Guidelines for the implementation of the H/V spectral ratio technique on ambient vibrations measurements, processing and interpretation. Bulletin of Earthquake Engineering 6, 1–2.

Capon, J., 1969. High-resolution frequency-wavenumber spectrum analysis. Proc. IEEE 57, 1408–1418. https://doi.org/10.1109/PROC.1969.7278

Department of Earth and Environmental Sciences, Geophysical Observatory, University of Munchen, 2001. BayernNetz (BH) seismic network. International Federation of Digital Seismograph Networks. https://doi.org/10.7914/SN/BW

Johnson, D.H., Dudgeon, D.E., 1993. Array Signal Processing: Concepts and Techniques, Facsimile Edition. ed. Prentice Hall, Englewood Cliffs, NJ.

Kristeková, M., Kristek, J., Moczo, P., 2009. Time-frequency misfit and goodness-of-fit criteria for quantitative comparison of time signals. Geophysical Journal International 178, 813–825. https://doi.org/10.1111/j.1365-246X.2009.04177.x

Kristekova, M., Kristek, J., Moczo, P., Day, S.M., 2006. Misfit Criteria for Quantitative Comparison of Seismograms. Bulletin of the Seismological Society of America 96, 1836–1850. https://doi.org/10.1785/0120060012

Lindsey, N.J., Rademacher, H., Ajo-Franklin, J.B., 2020. On the Broadband Instrument Response of Fiber-Optic DAS Arrays. J. Geophys. Res. Solid Earth 125. https://doi.org/10.1029/2019JB018145

Luu, K., 2020. disba - PyPI [WWW Document]. disba 0.6.1. URL https://pypi.org/project/disba/

Nakamura, Y., 2000. Clear identification of fundamental idea of Nakamura's technique and its applications. Proceedings of the XII World Conference Earthquake Engineering Paper no 2656.

Nogoshi, M., Igarashi, T., 1971. On the Amplitude Characteristics of Microtremor (Part 2). Zisin (Journal of the Seismological Society of Japan. 2nd ser.) 24, 26–40. https://doi.org/10.4294/zisin1948.24.1_26

Peterson, J.R., 1993. Observations and modeling of seismic background noise (No. 93–322), Open-File Report. U.S. Geological Survey. https://doi.org/10.3133/ofr93322

Rost, S., Thomas, C., 2002. Array Seismology: Methods and Applications. Reviews of Geophysics 40, 2-1-2–27. https://doi.org/10.1029/2000RG000100

Schweitzer, J., Fyen, J., Mykkeltveit, S., Gibbons, S.J., Pirli, M., Kühn, D., Kværna, T., 2012. Seismic Arrays. New Manual of Seismological Observatory Practice 2 (NMSOP2) 6 mb, 80 pages. https://doi.org/10.2312/GFZ.NMSOP-2_CH9

Wathelet, M., Chatelain, J.-L., Cornou, C., Giulio, G.D., Guillier, B., Ohrnberger, M., Savvaidis, A., 2020. Geopsy: A User-Friendly Open-Source Tool Set for Ambient Vibration Processing. Seismological Research Letters 91, 1878–1889. https://doi.org/10.1785/0220190360